Torsional selection rules, Raman tensors, and cross sections for degenerate modes of C_2H_6

J. M. Fernández[a] and S. Montero
Instituto de Estructura de la Materia, CSIC, Serrano 121, 28006 Madrid, Spain

(Received 14 October 2002; accepted 14 November 2002)

We analyze the peculiarities induced by the torsional motion on the Raman spectra of the degenerate vibrational bands of ethane. Selection rules for the Raman transitions between the torsionally split energy levels are derived first in terms of symmetry arguments. Then, their associated intensities are calculated with a model for the torsional dependence of the molecular polarizability. New experimental spectra of the Raman degenerate bands of C_2H_6, some recorded in jet expansions, are also included and analyzed to show the current state of the problem. © *2003 American Institute of Physics.* [DOI: 10.1063/1.1535420]

I. INTRODUCTION

Ethane is a prototype molecule for the study of torsion, a sort of internal motion of remarkable complexity. Unlike rotation or vibration, the wave functions associated with torsion cannot be described in terms of simple analytical functions. Instead, Fourier series are required, often with a slow convergence. The torsional energy spectrum lacks from the regularities of the rigid rotor or harmonic oscillator approximations, and, in addition, the torsional periodic potential leads to tunnel splittings. Consequently, the fine structure of the spectra of molecules with torsional degrees of freedom is far more complex than that of semirigid molecules.

Ethane has a ''moderate'' ($\sim$1000 cm^{-1}) barrier to internal rotation. Thus, its torsional motion behaves, at low excitation, close to a vibrational mode. The torsional amplitude, however, increases rapidly with excitation, leading to increasingly larger splittings of the torsional sublevels. Hence, the vibrational infrared and Raman spectra of fundamental bands look at low resolution similar to those of semirigid molecules, and can thus be interpreted to a first approximation by means of a staggered molecular configuration of D_{3d} symmetry. But, at resolution high enough to reveal the tunneling splittings, the theoretical methods of nonrigid molecules become necessary for the interpretation of the wave numbers and intensities of the rotation/torsional fine structure. In particular, the permutation-inversion G_{36}^{+} double group is necessary to account for perturbations of torsional nature which are allowed in floppy (G_{36}^{+}) ethane but have no equivalence in semirigid (D_{3d}) ethane. For all these reasons, the interpretation of the vibrational bands of ethane has progressed slowly compared to other semirigid molecules of similar size.

Among the 11 fundamental (genuine) vibrations of C_2H_6, just the two lowest frequency bands, the IR[1–4] $\nu_9(E_{1d})=821.74\,cm^{-1}$, and the Raman[4,5] $\nu_3(A_{1s})=994.1108\,cm^{-1}$ bands have been so far analyzed in detail. The IR bands $\nu_6(A_{4s})=1379.163\,cm^{-1}$ and $\nu_8(E_{1d})=1471.634\,cm^{-1}$, although analyzed,[6,7] show a number of perturbations not yet accounted for satisfactorily. The high-resolution IR spectra of $\nu_5(A_{4s})=2895.67\,cm^{-1}$ and $\nu_7(E_{1d})=2985.39\,cm^{-1}$, partly assigned[8] and analyzed,[9–11] are strongly perturbed. The low-resolution Raman spectra of $\nu_{10}(E_{2d})=2968.69\,cm^{-1}$ and $\nu_{11}(E_{2d})=1468.1\,cm^{-1}$ have been analyzed in the frame of a semirigid molecule model,[12] and the extremely weak[13] $\nu_{12}(E_{2d})$ fundamental has been reported at about 1196 cm^{-1} without any further interpretation.[14,15] The high-resolution Raman spectra of the highly perturbed Fermi multiplet, $\nu_u=2951.501/2957.89\,cm^{-1}$ and $\nu_l=2897.204\,cm^{-1}$, related to the fundamental $\nu_1(A_{1s})$, has been the subject of a preliminary analysis.[16] The remaining fundamental $\nu_2(A_{1s})=1397\,cm^{-1}$, though Raman allowed, is very weak and appears overlapped by the much stronger rotational structure of $\nu_{11}(E_{2d})$; its wave number is indirectly known from the $\nu_2-\nu_3$ difference band.[17]

In addition to these 11 fundamental bands, the torsional combinations $\nu_{11}+\nu_4$ and $\nu_{12}+\nu_4$ have been partially analyzed,[6,18] and several other overtones, combinations, and difference bands have been reported.[8,15,19–23] In turn, vibrational intensities of ethane have received much less attention: Raman[13,24] and IR intensities[25] have been interpreted by means of parametric descriptions and by *ab initio* methods[26] in the frame of a semirigid model.

Many spectral peculiarities of ethane related with the torsional motion have been considered in the cited literature, or in several relevant theoretical works.[27–30] The torsional Raman[17,31] and IR[32] spectra of ethane, including its intensities,[33] have been analyzed in detail. Other aspects, like the rotation–torsion–vibration Raman selection rules of ethanelike molecules,[29] or the torsional dependence of Raman tensors, though recognized long ago,[34] have not been treated before in much detail. The main purpose of the present work is to show the peculiarities induced by the torsional motion on the Raman spectra of the degenerate vibrational bands of ethane. Eventually, we intend to trace, through the Raman intensities, the conceptual transition from D_{3d} description of ethane to the G_{36}^{+} one. This leads to some

[a]Electronic mail: jmfernandez@iem.cfmac.csic.es

interesting relations between the intensities of degenerate bands related by an arbitrary torsional excitation. Some new experimental material is also included to illustrate the state of the art of the problem.

II. THEORY

A. Raman cross sections and selection rules

The vibrational–torsional–rotational energy levels of ethane will be denoted as (V,T,R), where $V=\{v_1v_2v_3v_5v_6v_7^{l_7}v_8^{l_8}v_9^{l_9}v_{10}^{l_{10}}v_{11}^{l_{11}}v_{12}^{l_{12}}\}$ stands for the set of vibrational quantum numbers, $T=\{v_4\sigma\}$ for the torsional quantum number v_4, and its symmetry label $\sigma=A_{1s}$, E_{3d}, E_{3s}, A_{3d} for $v_4=$even, or $\sigma=A_{1d}$, E_{3s}, E_{3d}, A_{3s} for $v_4=$odd; $R=\{Jk\}$ are the symmetric top rotational quantum numbers other than m.

Under a 90° scattering geometry $[X(MN)Z]$, with $MN=YY$, or $MN=YX$, the differential Raman cross section for a transition between two vibrational–torsional–rotational levels of ethane, of energies E_{VTR} and $E_{V'T'R'}$ and wave functions $|VTR\rangle$ and $|V'T'R'\rangle$, is given by

$$\left(\frac{\partial\sigma}{\partial\Omega}\right)^{[X(MN)Z]}_{|VTR\rangle\rightarrow|V'T'R'\rangle}=\left(\frac{\pi}{\epsilon_0}\right)^2(\nu_0-\nu)^4\frac{g_{VTR}e^{-E_{VTR}/k_B\Theta}}{Z(\Theta)}\times S^{[MN]}_{(VTR\rightarrow V'T'R')}, \tag{1}$$

expression valid under the usual conditions of nonresonant excitation of Raman scattering, assuming the gas sample to be in thermal equilibrium at the temperature Θ; $\epsilon_0=8.854\,19\cdot10^{-12}\,\mathrm{CV^{-1}\,m^{-1}}$ is the permittivity of vacuum, ν_0 the wave number of the exciting radiation, $\nu=(E_{V'T'R'}-E_{VTR})/hc$ the wave number of the Raman shift, and g_{VTR} the statistical weight of $|VTR\rangle$ due to nuclear spin degeneracy; k_B is Boltzmann's constant, $Z(\Theta)$ the partition function at the temperature Θ, and

$$S^{[MN]}_{(VTR\rightarrow V'T'R')}=\delta_{MN}\frac{\delta_{JJ'}\delta_{kk'}}{3}(2J+1)\langle V'T'|\alpha_0^{(0)}|VT\rangle^2+\frac{3+\delta_{MN}}{30}(2J+1)(2J'+1)\times\begin{pmatrix}J' & 2 & J\\ -k' & \tau & k\end{pmatrix}^2|\langle V'T'|\alpha_\tau^{(2)}|VT\rangle|^2 \tag{2}$$

the scattering strength for the irreducible component $\alpha_\tau^{(\ell)}$ of the molecular polarizability tensor, with $\tau=\Delta k=k'-k$.

Equations (1) and (2) hold for an exciting wave number ν_0 far from resonant conditions. The molecular polarizability tensor may then be considered symmetric, and its spherically irreducible components $\alpha_\tau^{(\ell)}$ in Eq. (2) become

$$\begin{aligned}\alpha_0^{(0)}&=-(\alpha_{xx}+\alpha_{yy}+\alpha_{zz})/\sqrt{3},\\ \alpha_0^{(2)}&=(2\alpha_{zz}-\alpha_{xx}-\alpha_{yy})/\sqrt{6},\\ \alpha_{\pm1}^{(2)}&=\mp\alpha_{xz}-i\alpha_{yz},\\ \alpha_{\pm2}^{(2)}&=(\alpha_{xx}-\alpha_{yy})/2\pm i\alpha_{xy},\end{aligned} \tag{3}$$

when expressed in terms of the Cartesian elements.

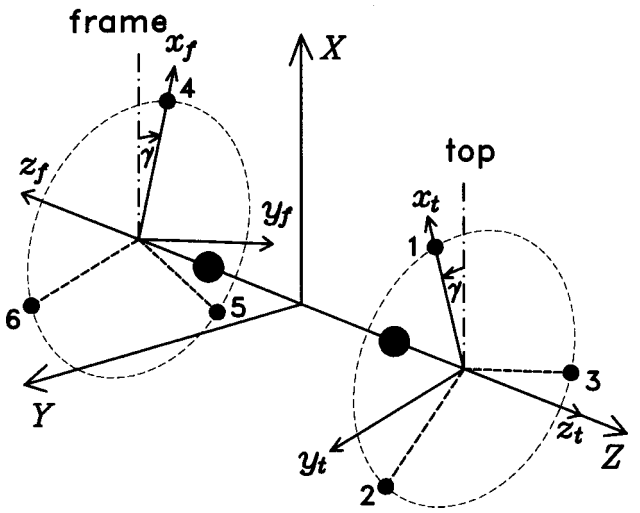

FIG. 1. Local axis system of the top (x_t,y_t,z_t), frame (x_f,y_f,z_f), and molecular axis system (X,Y,Z) of ethane, and definition of torsional angle γ used in the present work.

From Eq. (2) it can be noticed that rotational selection rules are determined by the nonvanishing conditions of the 3-j symbol, while the vibrational and torsional selection rules come altogether from the $\langle V'T'|\alpha_\tau^{(\ell)}|VT\rangle$ transition moments. In semirigid molecules the elements $\alpha_\tau^{(\ell)}$ depend only on the normal coordinates, q, but in ethane they are functions simultaneously of the q's, and of the torsional coordinate γ, defined in Fig. 1. This difference has important consequences, for the resulting Raman selection rules are not the same in the D_{3d} point group (semirigid molecule) than in the G_{36}^+ double group (floppy molecule).

The vibrational and torsional selection rules for the G_{36}^+ group may be derived with aid of the power series expansion

$$\alpha_\tau^{(\ell)}(q,\gamma)=(\alpha_\tau^{(\ell)})_\gamma+\left(\frac{\partial\alpha_\tau^{(\ell)}}{\partial q_i}\right)_\gamma q_i+\frac{1}{2}\left(\frac{\partial^2\alpha_\tau^{(\ell)}}{\partial q_i\partial q_j}\right)_\gamma q_iq_j+\cdots, \tag{4}$$

in terms of the $3N-7=17$ vibrational normal coordinates (dimensionless) q_i defined below. In Eq. (4) the convention of summing over repeated subindices is implicit. The coefficients $(\alpha_\tau^{(\ell)})_\gamma$, $(\partial\alpha_\tau^{(\ell)}/\partial q_i)_\gamma$, and $(\partial^2\alpha_\tau^{(\ell)}/\partial q_i\partial q_j)_\gamma$, in the power series are functions of the torsional angle γ, a periodic variable. They may thus be expressed as a Fourier series of the generic form

$$(—)_\gamma=\sum_{n=0}^{\infty}C^{(n)}\cos n\gamma+\sum_{n=1}^{\infty}S^{(n)}\sin n\gamma. \tag{5}$$

Group theory establishes which coefficients $C^{(n)}$ or $S^{(n)}$ are nonzero by symmetry: For each particular derivative of the irreducible polarizability element, each term in the right-hand side of Eq. (4) must have the same symmetry as the left-hand side. This implies that

TABLE I. Symmetry of periodic functions $f(\gamma)$ [n mod 6] in G_{36}^{+}.

$f(\gamma)$	Γ	$f(\gamma)$	Γ
$\cos\gamma$	E_{3d}	$\sin\gamma$	E_{3d}
$\cos 2\gamma$	E_{3s}	$\sin 2\gamma$	E_{3s}
$\cos 3\gamma$	A_{1d}	$\sin 3\gamma$	A_{3d}
$\cos 4\gamma$	E_{3s}	$\sin 4\gamma$	E_{3s}
$\cos 5\gamma$	E_{3d}	$\sin 5\gamma$	E_{3d}
$\cos 6\gamma$	A_{1s}	$\sin 6\gamma$	A_{3s}

$$\begin{aligned}\Gamma(\alpha_\tau^{(\ell)}(q,\gamma)) &= \Gamma((\alpha_\tau^{(\ell)})_\gamma)\\ &= \Gamma\left(\left(\frac{\partial\alpha_\tau^{(\ell)}}{\partial q_i}\right)_\gamma\right)\otimes\Gamma(q_i)\\ &= \Gamma\left(\left(\frac{\partial^2\alpha_\tau^{(\ell)}}{\partial q_i\partial q_j}\right)_\gamma\right)\otimes\Gamma(q_iq_j).\end{aligned}\tag{6}$$

The allowed symmetries of the left-hand side on Eq. (6) are known from the character table[27] of the group G_{36}^{+}: $\Gamma(\alpha_0^{(0)})=A_{1s}$, $\Gamma(\alpha_0^{(2)})=A_{1s}$, $\Gamma(\alpha_{\pm1}^{(2)})=E_{2d}$, and $\Gamma(\alpha_{\pm2}^{(2)})=E_{1s}$. In turn, the symmetries of the functions $\cos n\gamma$ and $\sin n\gamma$, required for the full exploitation of Eq. (6), are given in Table I. On the other hand, the symmetry of the 17 normal coordinates q_i of C_2H_6 satisfies[29]

$$\begin{aligned}\Gamma_{VIB}(q_i) \in\ & 3A_{1s}\oplus 2A_{4s}\oplus(3-m)(E_{1s}\oplus E_{2s})\\ & \oplus m(E_{1d}\oplus E_{2d}),\end{aligned}\tag{7}$$

with $m=0$, 1, 2, or 3, not fixed *a priori* by symmetry. With these constraints in mind, the periodic functional dependence of $(\partial\alpha_\tau^{(\ell)}/\partial q_i)_\gamma$, and $(\partial^2\alpha_\tau^{(\ell)}/\partial q_i\partial q_j)_\gamma$ on the torsional angle is deduced from the symmetry compatibility Eq. (6). The result is summarized in Table II.

The degenerate vibrations of ethanelike molecules can be seen to occur into "pairs" of analog motions,[35] close in frequency; in C_2H_6 they are: the two asymmetric CH stretchings ν_7 and ν_{10}, the two asymmetric HCH bendings ν_8 and ν_{11}, and the two methyl rockings ν_9 and ν_{12}. One component of each pair is IR active and the other is Raman active in a semirigid model. Actually, the two components of the pair are combinations of degenerate vibrations of top and frame, one symmetric and the other antisymmetric with respect to the interchange of the two halves of the molecule.

It must be emphasized here that the symmetry of the degenerate normal coordinates of ethane cannot be determined unambiguously on the sole basis of symmetry arguments, a peculiarity of molecules with internal rotation. The choice between $(E_{1d}\oplus E_{2d})$ and $(E_{1s}\oplus E_{2s})$ in Eq. (7) depends on the vibrational potential function[36] or, to be more precise, on the way it changes with the torsional angle. From the analysis of the subtle torsional splittings of the IR-active fundamentals of C_2H_6, the G_{36}^{+} symmetries

$$\begin{aligned}&\Gamma(q_7)=\Gamma(q_8)=\Gamma(q_9)=E_{1d},\\ &\Gamma(q_{10})=\Gamma(q_{11})=\Gamma(q_{12})=E_{2d},\end{aligned}\tag{8}$$

have been proposed[37] for the six degenerate normal coordinates of C_2H_6. These symmetries will be used throughout this paper.

Substituting the power series expansion (4) into Eq. (2), and taking account of Table II, the vibrational–torsional selection rules are obtained from the condition

$$\begin{aligned}&\langle V'T'|\alpha_\tau^{(\ell)}|VT\rangle\neq 0,\\ &\text{if}\ \ \Gamma(|VT\rangle)\otimes\Gamma(\alpha_\tau^{(\ell)})\otimes\Gamma(|V'T'\rangle)\ni A_{1s}.\end{aligned}\tag{9}$$

The resulting 32 vibrational–torsional–rotational selection rules for Raman transitions involving degenerate modes, and an arbitrary number of torsional excitation, are summarized in Table III. The transition patterns emerging from these selection rules are intricate and do not seem amenable to further simplification. Indeed, the actual transition patterns are still more involved due to the ζ^z–Coriolis splitting of the double degenerate vibrational levels.

Figure 2 displays the scheme of rotation–torsional energy levels for degenerate vibrational states of E_{1d} and E_{2d} symmetry, and arbitrary torsional excitations. For every vibrational–torsional–rotational energy level (solid lines), the following symmetries are given: symmetry of the torsional wave function Γ_{TOR} in the left column, symmetry of the rotational wave function Γ_{ROT} on the bottom line, and

TABLE II. Torsional dependence of the first and second derivatives of the irreducible components of the molecular polarizability tensor of ethane with respect to the normal coordinates q_i.

Sym $\Gamma(q_i)$	Polarizability 1st derivative	Sym $\Gamma(q_iq_j)$	Polarizability 2nd derivative
A_{1s}	$(\partial\alpha_0^{(0)}/\partial q_i)_\gamma\propto\cos 6n\gamma$	A_{1s}	$(\partial^2\alpha_0^{(0)}/\partial q_i\partial q_j)_\gamma\propto\cos 6n\gamma$
A_{1s}	$(\partial\alpha_0^{(2)}/\partial q_i)_\gamma\propto\cos 6n\gamma$	A_{1s}	$(\partial^2\alpha_0^{(2)}/\partial q_i\partial q_j)_\gamma\propto\cos 6n\gamma$
		A_{3s}	$(\partial^2\alpha_0^{(0)}/\partial q_i\partial q_j)_\gamma\propto\sin 6n\gamma$
		A_{3s}	$(\partial^2\alpha_0^{(2)}/\partial q_i\partial q_j)_\gamma\propto\sin 6n\gamma$
E_{1d}	$(\partial\alpha_{\pm1}^{(2)}/\partial q_i)_\gamma\propto\sin 6n\gamma$	E_{1d}	$(\partial^2\alpha_{\pm1}^{(2)}/\partial q_i\partial q_j)_\gamma\propto\sin 6n\gamma$
E_{1d}	$(\partial\alpha_{\pm2}^{(2)}/\partial q_i)_\gamma\propto\cos(6n+3)\gamma$	E_{1d}	$(\partial^2\alpha_{\pm2}^{(2)}/\partial q_i\partial q_j)_\gamma\propto\cos(6n+3)\gamma$
E_{2d}	$(\partial\alpha_{\pm1}^{(2)}/\partial q_i)_\gamma\propto\cos 6n\gamma$	E_{2d}	$(\partial^2\alpha_{\pm1}^{(2)}/\partial q_i\partial q_j)_\gamma\propto\cos 6n\gamma$
E_{2d}	$(\partial\alpha_{\pm2}^{(2)}/\partial q_i)_\gamma\propto\sin(6n+3)\gamma$	E_{2d}	$(\partial^2\alpha_{\pm2}^{(2)}/\partial q_i\partial q_j)_\gamma\propto\sin(6n+3)\gamma$
E_{1s}	$(\partial\alpha_{\pm1}^{(2)}/\partial q_i)_\gamma\propto\sin(6n+3)\gamma$	E_{1s}	$(\partial^2\alpha_{\pm1}^{(2)}/\partial q_i\partial q_j)_\gamma\propto\sin(6n+3)\gamma$
E_{1s}	$(\partial\alpha_{\pm2}^{(2)}/\partial q_i)_\gamma\propto\cos 6n\gamma$	E_{1s}	$(\partial^2\alpha_{\pm2}^{(2)}/\partial q_i\partial q_j)_\gamma\propto\cos 6n\gamma$
E_{2s}	$(\partial\alpha_{\pm1}^{(2)}/\partial q_i)_\gamma\propto\cos(6n+3)\gamma$	E_{2s}	$(\partial^2\alpha_{\pm1}^{(2)}/\partial q_i\partial q_j)_\gamma\propto\cos(6n+3)\gamma$
E_{2s}	$(\partial\alpha_{\pm2}^{(2)}/\partial q_i)_\gamma\propto\sin 6n\gamma$	E_{2s}	$(\partial^2\alpha_{\pm2}^{(2)}/\partial q_i\partial q_j)_\gamma\propto\sin 6n\gamma$
		$n=0,1,2,...$	

TABLE III. Raman selection rules for $\Delta v_i=1$ vibrational–torsional–rotational transitions $|v_i=0,v_4\sigma\rangle\rightarrow|v_i=1,v_4'\sigma'\rangle$ of C_2H_6, involving a degenerate normal coordinate q_i of symmetry $\Gamma(q_i)$, and arbritrary torsional excitations v_4 and v_4'; $\Delta J=0,\pm1,\pm2$ for all transitions; $(\partial\alpha_\tau^{(\ell)}/\partial q_i)_\gamma$ is the polarizability component responsible for the Raman intensity, with its torsional dependence and symmetry in G_{36}^+ indicated in squared brackets; $e=even$, $o=odd$ parity.

$\Gamma(q_i)$	$(\partial\alpha_\tau^{(\ell)}/\partial q)_\gamma$	Δk	$v_4\rightarrow v_4'$	$\sigma\rightarrow\sigma'$	Num
E_{1d}	$(\partial\alpha_{\pm1}^{(2)}/\partial q)_\gamma$	±1	$e\ e$	$E_{3s}\rightarrow E_{3s}$; $E_{3d}\rightarrow E_{3d}$	1
	$[\sin 6n\gamma]$		$o\ e$	$E_{3s}\rightarrow E_{3s}$; $E_{3d}\rightarrow E_{3d}$; $A_{3s}\rightarrow A_{1s}$; $A_{1d}\rightarrow A_{3d}$	2
	$[A_{3s}]$		$e\ o$	$E_{3s}\rightarrow E_{3s}$; $E_{3d}\rightarrow E_{3d}$; $A_{1s}\rightarrow A_{3s}$; $A_{3d}\rightarrow A_{1d}$	3
			$o\ o$	$E_{3s}\rightarrow E_{3s}$; $E_{3d}\rightarrow E_{3d}$	4
	$(\partial\alpha_{\pm2}^{(2)}/\partial q)_\gamma$	±2	$e\ e$	$E_{3s}\rightarrow E_{3d}$; $E_{3d}\rightarrow E_{3s}$	5
	$[\cos(6n+3)\gamma]$		$o\ e$	$E_{3s}\rightarrow E_{3d}$; $E_{3d}\rightarrow E_{3s}$; $A_{3s}\rightarrow A_{3d}$; $A_{1d}\rightarrow A_{1s}$	6
	$[A_{1d}]$		$e\ o$	$E_{3s}\rightarrow E_{3d}$; $E_{3d}\rightarrow E_{3s}$; $A_{3d}\rightarrow A_{3s}$; $A_{1s}\rightarrow A_{1d}$	7
			$o\ o$	$E_{3s}\rightarrow E_{3d}$; $E_{3d}\rightarrow E_{3s}$	8
E_{2d}	$(\partial\alpha_{\pm1}^{(2)}/\partial q)_\gamma$	±1	$e\ e$	$E_{3s}\rightarrow E_{3s}$; $E_{3d}\rightarrow E_{3d}$; $A_{1s}\rightarrow A_{1s}$; $A_{3d}\rightarrow A_{3d}$	9
	$[\cos 6n\gamma]$		$o\ e$	$E_{3s}\rightarrow E_{3s}$; $E_{3d}\rightarrow E_{3d}$	10
	$[A_{1s}]$		$e\ o$	$E_{3s}\rightarrow E_{3s}$; $E_{3d}\rightarrow E_{3d}$	11
			$o\ o$	$E_{3s}\rightarrow E_{3s}$; $E_{3d}\rightarrow E_{3d}$; $A_{3s}\rightarrow A_{3s}$; $A_{1d}\rightarrow A_{1d}$	12
	$(\partial\alpha_{\pm2}^{(2)}/\partial q)_\gamma$	±2	$e\ e$	$E_{3s}\rightarrow E_{3d}$; $E_{3d}\rightarrow E_{3s}$; $A_{1s}\rightarrow A_{3d}$; $A_{3d}\rightarrow A_{1s}$	13
	$[\sin(6n+3)\gamma]$		$o\ e$	$E_{3s}\rightarrow E_{3d}$; $E_{3d}\rightarrow E_{3s}$	14
	$[A_{3d}]$		$e\ o$	$E_{3s}\rightarrow E_{3d}$; $E_{3d}\rightarrow E_{3s}$	15
			$o\ o$	$E_{3s}\rightarrow E_{3d}$; $E_{3d}\rightarrow E_{3s}$; $A_{3s}\rightarrow A_{1d}$; $A_{1d}\rightarrow A_{3s}$	16
E_{1s}	$(\partial\alpha_{\pm1}^{(2)}/\partial q)_\gamma$	±1	$e\ e$	$E_{3s}\rightarrow E_{3d}$; $E_{3d}\rightarrow E_{3s}$; $A_{1s}\rightarrow A_{3d}$; $A_{3d}\rightarrow A_{1s}$	17
	$[\sin(6n+3)\gamma]$		$o\ e$	$E_{3s}\rightarrow E_{3d}$; $E_{3d}\rightarrow E_{3s}$	18
	$[A_{3d}]$		$e\ o$	$E_{3s}\rightarrow E_{3d}$; $E_{3d}\rightarrow E_{3s}$	19
			$o\ o$	$E_{3s}\rightarrow E_{3d}$; $E_{3d}\rightarrow E_{3s}$; $A_{3s}\rightarrow A_{1d}$; $A_{1d}\rightarrow A_{3s}$	20
	$(\partial\alpha_{\pm2}^{(2)}/\partial q)_\gamma$	±2	$e\ e$	$E_{3s}\rightarrow E_{3s}$; $E_{3d}\rightarrow E_{3d}$; $A_{1s}\rightarrow A_{1s}$; $A_{3d}\rightarrow A_{3d}$	21
	$[\cos 6n\gamma]$		$o\ e$	$E_{3s}\rightarrow E_{3s}$; $E_{3d}\rightarrow E_{3d}$	22
	$[A_{1s}]$		$e\ o$	$E_{3s}\rightarrow E_{3s}$; $E_{3d}\rightarrow E_{3d}$	23
			$o\ o$	$E_{3s}\rightarrow E_{3s}$; $E_{3d}\rightarrow E_{3d}$; $A_{3s}\rightarrow A_{3s}$; $A_{1d}\rightarrow A_{1d}$	24
E_{2s}	$(\partial\alpha_{\pm1}^{(2)}/\partial q)_\gamma$	±1	$e\ e$	$E_{3s}\rightarrow E_{3d}$; $E_{3d}\rightarrow E_{3s}$	25
	$[\cos(6n+3)\gamma]$		$o\ e$	$E_{3s}\rightarrow E_{3d}$; $E_{3d}\rightarrow E_{3s}$; $A_{3s}\rightarrow A_{3d}$; $A_{1d}\rightarrow A_{1s}$	26
	$[A_{1d}]$		$e\ o$	$E_{3s}\rightarrow E_{3d}$; $E_{3d}\rightarrow E_{3s}$; $A_{3d}\rightarrow A_{3s}$; $A_{1s}\rightarrow A_{1d}$	27
			$o\ o$	$E_{3s}\rightarrow E_{3d}$; $E_{3d}\rightarrow E_{3s}$	28
	$(\partial\alpha_{\pm2}^{(2)}/\partial q)_\gamma$	±2	$e\ e$	$E_{3s}\rightarrow E_{3s}$; $E_{3d}\rightarrow E_{3d}$	29
	$[\sin 6n\gamma]$		$o\ e$	$E_{3s}\rightarrow E_{3s}$; $E_{3d}\rightarrow E_{3d}$; $A_{3s}\rightarrow A_{1s}$; $A_{1d}\rightarrow A_{3d}$	30
	$[A_{3s}]$		$e\ o$	$E_{3s}\rightarrow E_{3s}$; $E_{3d}\rightarrow E_{3d}$; $A_{1s}\rightarrow A_{3s}$; $A_{3d}\rightarrow A_{1d}$	31
			$o\ o$	$E_{3s}\rightarrow E_{3s}$; $E_{3d}\rightarrow E_{3d}$	32

symmetry of the total vibrational–torsional–rotational wave function Γ_{VTR} on top of each level, along with its statistical weight (in parentheses) for $^{12}C_2H_6$. Dotted lines represent nonacceptable combinations of rotational and torsional wave functions, and are depicted only to show the staggering of torsional levels for different parities of k.

It should be noticed that the same four schemes of Fig. 2 would occur if the symmetry of the pair of vibrational coordinates were $E_{1s}+E_{2s}$ instead of $E_{1d}+E_{2d}$, but rearranged this way: (a) E_{1s}, $v_4=$even; (b) E_{1s}, $v_4=$odd; (c) E_{2s}, $v_4=$even; and (d) E_{2s}, $v_4=$odd; i.e., the even/odd character of v_4 is reversed in going from a E_d vibrational symmetry to a E_s one. Thus, in practical terms, the main difference between an $E_{1s}+E_{2s}$ pair and an $E_{1d}+E_{2d}$ one is the ordering of the torsional splittings. This property was used[37] in the IR spectrum to determine the symmetry in G_{36}^+ of the 6 degenerate vibrations of C_2H_6.

In Fig. 3, the $\Delta k=\pm1$ and $\Delta k=\pm2$ Raman active transitions of a fundamental band of E_{2d} symmetry are shown. It can be noticed in Fig. 3(a) that $\Delta k=\pm1$ transitions always connect states with the *same torsional* wave functions. Thus, the torsional splitting of a vibrotational transition is the *difference* of the torsional splittings of the initial and final states. On the contrary, in Fig. 3(b), the $\Delta k=\pm2$ transitions connect the lower component of the torsional manifold in the initial state with the upper one in the final; thus, the torsional splitting of the transition is the *sum* of the torsional splittings of the involved vibrational states. Figures 3(a) and 3(b) display, respectively, the selection rules number 9 and 13 of Table III.

B. Torsional-dependent Raman tensors

The selection rules on Table III state whether a particular vibrational–torsional–rotational transition is allowed by symmetry, but do not provide any clue about the expected intensity. According to Eqs. (1)–(4), this information can only be deduced from the quantities $(\alpha_\tau^{(\ell)})_\gamma$ for transitions within the same vibrational state, from $(\partial\alpha_\tau^{(\ell)}/\partial q_i)_\gamma$ for a fundamental transition, and from $(\partial^2\alpha_\tau^{(\ell)}/\partial q_i\partial q_j)_\gamma$, for an overtone or combination transition. A procedure to calculate the first derivatives of the torsional-dependent Raman tensors is described next.

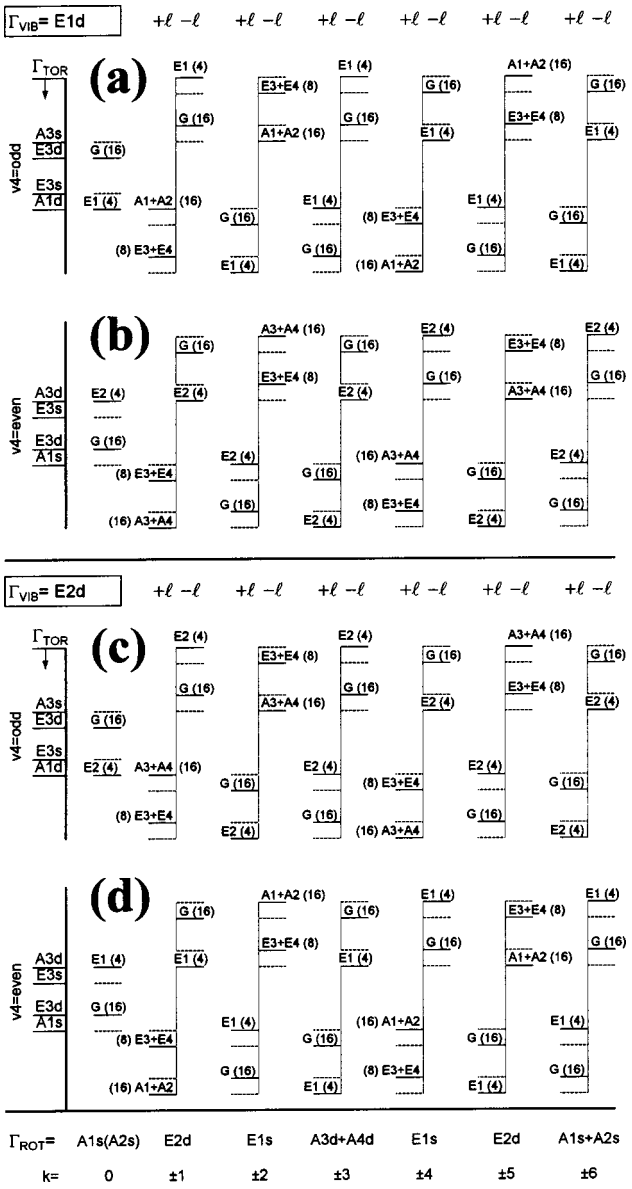

FIG. 2. Rotational–torsional level scheme of ethane for a degenerate vibrational level of symmetry Γ_{vib}. The ordering of the $+\ell$ and $-\ell$ components of the z-Coriolis splitting shown here is for $\zeta^z>0$; for $\zeta^z<0$ this order is reversed. For the notation of vibrational–torsional–rotational energy levels and z-Coriolis splittings, see the text. These schemes also hold for vibrational symmetries E_{1s} and E_{2s} with the following correspondence: (a) $\Gamma_{vib}=E_{1s}$, $v_4=$even; (b) $\Gamma_{vib}=E_{1s}$, $v_4=$odd; (c) $\Gamma_{vib}=E_{2s}$, $v_4=$even; (d) $\Gamma_{vib}=E_{2s}$, $v_4=$odd.

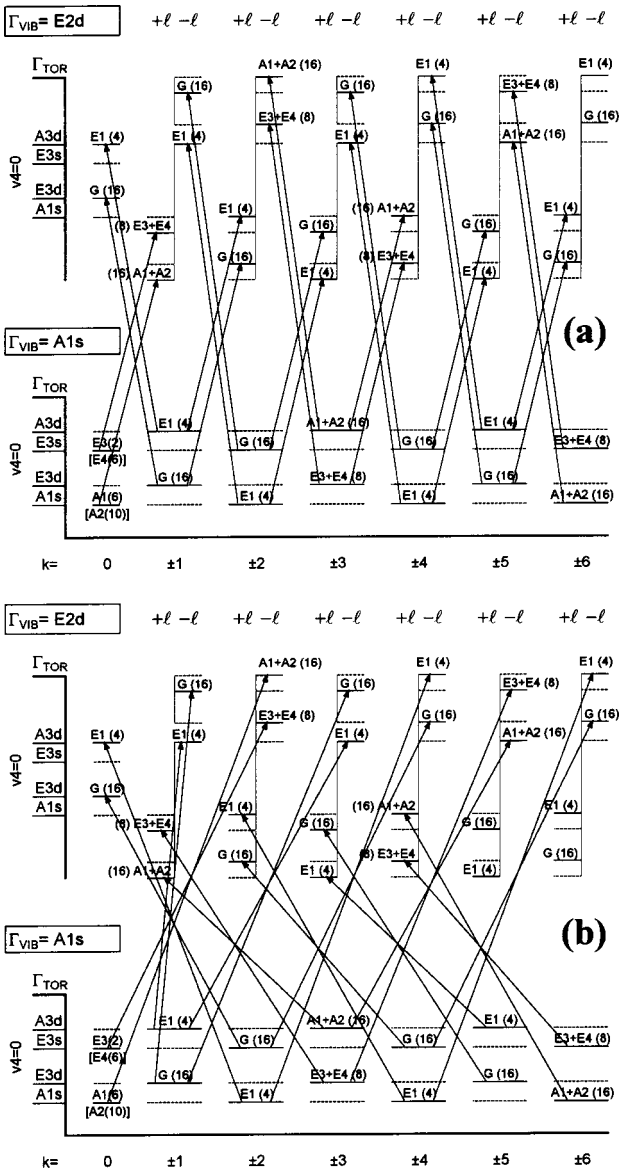

FIG. 3. Raman transitions from the ground to a $\Gamma_{vib}=E_{2d}$ vibrational state. (a) $\Delta k=\pm 1$ transitions; (b) $\Delta k=\pm 2$ transitions. For the notation of vibrational–torsional–rotational energy levels and z-Coriolis splittings see the text and caption to Fig. 2.

For convenience, the problem of obtaining the numerical values of $(\partial\alpha_\tau^{(\ell)}/\partial q_i)_\gamma$'s will be carried out in two steps. First, the derivatives $(\partial\alpha_\tau^{(\ell)}/\partial S)_\gamma$ will be obtained with respect to a set of symmetry coordinates S. Subsequently, these derivatives will be transformed into the $(\partial\alpha_\tau^{(\ell)}/\partial q_i)_\gamma$'s by means of the vibrational eigenvector transformation described below.

1. Raman tensors in symmetry coordinates representation

For the purpose of modeling the molecular polarizability tensor (α) of ethane, we shall consider it as the sum of the contributions from two identical fragments of local symmetry C_{3v}. One fragment (t) stands for the *top* of the molecule, and the other (f), for the *frame*. This additivity may be expressed as

$$\alpha=\mathbf{T}_t^+\alpha_t\mathbf{T}_t+\mathbf{T}_f^+\alpha_f\mathbf{T}_f, \tag{10}$$

where α_t and α_f are the polarizability tensors of the fragments, referred to their local axis systems (x_t,y_t,z_t) and (x_f,y_f,z_f), shown in Fig. 1; $\mathbf{T}_t$ and $\mathbf{T}_f$, defined as

$$\mathbf{T}_t=\begin{pmatrix}\cos\gamma & \sin\gamma & 0\\ -\sin\gamma & \cos\gamma & 0\\ 0 & 0 & 1\end{pmatrix},$$
$$\mathbf{T}_f=\begin{pmatrix}\cos\gamma & -\sin\gamma & 0\\ -\sin\gamma & -\cos\gamma & 0\\ 0 & 0 & -1\end{pmatrix}, \tag{11}$$

TABLE IV. Symmetry coordinates for degenerate modes of ethane; $a=1$ Å is a length scaling factor.

$S_{7a}(E_{1d})=(1/\sqrt{2})[(cr_{tx}-sr_{ty})+(cr_{fx}-sr_{fy})]$
$S_{7b}(E_{1d})=(1/\sqrt{2})[(sr_{tx}+cr_{ty})-(sr_{fx}+cr_{fy})]$
$S_{8a}(E_{1d})=(1/\sqrt{2})[(c\alpha_{tx}-s\alpha_{ty})+(c\alpha_{fx}-s\alpha_{fy})]$
$S_{8b}(E_{1d})=(1/\sqrt{2})[(s\alpha_{tx}+c\alpha_{ty})-(s\alpha_{fx}+c\alpha_{fy})]$
$S_{9a}(E_{1d})=(1/\sqrt{2})[(c\beta_{tx}-s\beta_{ty})+(c\beta_{fx}-s\beta_{fy})]$
$S_{9b}(E_{1d})=(1/\sqrt{2})[(s\beta_{tx}+c\beta_{ty})-(s\beta_{fx}+c\beta_{fy})]$

$S_{10a}(E_{2d})=(1/\sqrt{2})[(sr_{tx}+cr_{ty})+(sr_{fx}+cr_{fy})]$
$S_{10b}(E_{2d})=(1/\sqrt{2})[(-cr_{tx}+sr_{ty})+(cr_{fx}-sr_{fy})]$
$S_{11a}(E_{2d})=(1/\sqrt{2})[(s\alpha_{tx}+c\alpha_{ty})+(s\alpha_{fx}+c\alpha_{fy})]$
$S_{11b}(E_{2d})=(1/\sqrt{2})[(-c\alpha_{tx}+s\alpha_{ty})+(c\alpha_{fx}-s\alpha_{fy})]$
$S_{12a}(E_{2d})=(1/\sqrt{2})[(s\beta_{tx}+c\beta_{ty})+(s\beta_{fx}+c\beta_{fy})]$
$S_{12b}(E_{2d})=(1/\sqrt{2})[(-c\beta_{tx}+s\beta_{ty})+(c\beta_{fx}-s\beta_{fy})]$

$c=\cos\gamma$, $s=\sin\gamma$

$r_{tx}=(1/\sqrt{6})(2\delta r_1-\delta r_2-\delta r_3)$	$r_{ty}=(1/\sqrt{2})(\delta r_2-\delta r_3)$
$r_{fx}=(1/\sqrt{6})(2\delta r_4-\delta r_5-\delta r_6)$	$r_{fy}=(1/\sqrt{2})(\delta r_5-\delta r_6)$
$\alpha_{tx}=(a/\sqrt{6})(2\delta\alpha_1-\delta\alpha_2-\delta\alpha_3)$	$\alpha_{ty}=(a/\sqrt{2})(\delta\alpha_2-\delta\alpha_3)$
$\alpha_{fx}=(a/\sqrt{6})(2\delta\alpha_4-\delta\alpha_5-\delta\alpha_6)$	$\alpha_{fy}=(a/\sqrt{2})(\delta\alpha_5-\delta\alpha_6)$
$\beta_{tx}=(a/\sqrt{6})(2\delta\beta_1-\delta\beta_2-\delta\beta_3)$	$\beta_{ty}=(a/\sqrt{2})(\delta\beta_2-\delta\beta_3)$
$\beta_{fx}=(a/\sqrt{6})(2\delta\beta_4-\delta\beta_5-\delta\beta_6)$	$\beta_{fy}=(a/\sqrt{2})(\delta\beta_5-\delta\beta_6)$

δr_i=C–H_i stretching; $\delta\alpha_i$=H_j–C–H_k bending; $\delta\beta_i$=C–C–H_i bending

are the direction cosines matrices between the local axis systems of the fragments top and frame, and the molecule fixed system (X,Y,Z). It should be noted that orientation of the local axis systems used here (Fig. 1) differs from that used in the literature[29,30,36] in order to preserve formally the equivalence of the tensorial properties of the two fragments, like the polarizability.

The derivatives of the molecular polarizability with respect to the symmetry coordinates S of Table IV may then be expressed as

$$\frac{\partial\alpha}{\partial S}=\mathbf{T}_t^+\frac{\partial\alpha_t}{\partial S}\mathbf{T}_t+\mathbf{T}_f^+\frac{\partial\alpha_f}{\partial S}\mathbf{T}_f. \tag{12}$$

For the present purpose, $\partial\alpha_t/\partial S$ and $\partial\alpha_f/\partial S$ must be expressed in terms of the internal coordinates $(r_{tx},r_{ty},r_{fx},r_{fy})$, $(\alpha_{tx},\alpha_{ty},\alpha_{fx},\alpha_{fy})$, $(\beta_{tx},\beta_{ty},\beta_{fx},\beta_{fy})$ of the two fragments of the molecule, defined at the bottom of Table IV. For instance, for the derivatives of the polarizability of the fragment ''top'' with respect to any of the symmetry coordinates S_{7a}, S_{7b}, S_{10a}, or S_{10b}, which depend on the C–H stretching coordinates r's, we have

$$\frac{\partial\alpha_t}{\partial S}=\frac{\partial\alpha_t}{\partial r_{tx}}\frac{\partial r_{tx}}{\partial S}+\frac{\partial\alpha_t}{\partial r_{ty}}\frac{\partial r_{ty}}{\partial S}+\frac{\partial\alpha_t}{\partial r_{fx}}\frac{\partial r_{fx}}{\partial S}+\frac{\partial\alpha_t}{\partial r_{fy}}\frac{\partial r_{fy}}{\partial S}, \tag{13}$$

and similar expressions for the derivatives $\partial\alpha_f/\partial S$ of the fragment ''frame.'' The last two terms in Eq. (13) mixing the derivative of the top with a coordinate of the frame may be neglected because they are expected to be very small. Expressions analogous to that in Eq. (13) hold for the frame and for the other symmetry coordinates of Table IV depending on the H–C–H bendings (α's), and on the H–C–C bendings (β's).

The internal coordinates r_{tj}'s, α_{tj}'s, β_{tj}'s and r_{fj}'s, α_{fj}'s, β_{fj}'s, with $j=x,y$, defined at the bottom of Table IV have been chosen in such a way that they are well-oriented pairs of degenerate E-symmetry coordinates in the methyl groups. Thus, the local Raman tensors for the top and frame methyl groups are

$$\frac{\partial\alpha_t}{\partial r_{tx}}=\frac{\partial\alpha_f}{\partial r_{fx}}=\begin{pmatrix} d_r & 0 & e_r \\ 0 & -d_r & 0 \\ e_r & 0 & 0 \end{pmatrix}, \tag{14}$$

$$\frac{\partial\alpha_t}{\partial r_{ty}}=\frac{\partial\alpha_f}{\partial r_{fy}}=\begin{pmatrix} 0 & -d_r & 0 \\ -d_r & 0 & e_r \\ 0 & e_r & 0 \end{pmatrix}, \tag{15}$$

for the stretching coordinates, and similar ones for the bending coordinates, α_{tj}'s, β_{tj}'s and α_{fj}'s, β_{fj}'s defined in Table IV, replacing r by α, or by β.

Introducing the coefficients of the symmetry coordinates S_i of Table IV into Eqs. (13)–(15), the Raman tensors for the whole molecule

$$\frac{\partial\alpha}{\partial S_{ja}(E_{1d})}=\sqrt{2}\begin{pmatrix} d_\eta\cos 3\gamma & 0 & 0 \\ 0 & -d_\eta\cos 3\gamma & 0 \\ 0 & 0 & 0 \end{pmatrix},$$

$$\frac{\partial\alpha}{\partial S_{jb}(E_{1d})}=\sqrt{2}\begin{pmatrix} 0 & -d_\eta\cos 3\gamma & 0 \\ -d_\eta\cos 3\gamma & 0 & 0 \\ 0 & 0 & 0 \end{pmatrix}, \tag{16}$$

$$\frac{\partial\alpha}{\partial S_{la}(E_{2d})}=\sqrt{2}\begin{pmatrix} d_\eta\sin 3\gamma & 0 & 0 \\ 0 & -d_\eta\sin 3\gamma & e_\eta \\ 0 & e_\eta & 0 \end{pmatrix},$$

$$\frac{\partial\alpha}{\partial S_{lb}(E_{2d})}=\sqrt{2}\begin{pmatrix} 0 & -d_\eta\sin 3\gamma & -e_\eta \\ -d_\eta\sin 3\gamma & 0 & 0 \\ -e_\eta & 0 & 0 \end{pmatrix} \tag{17}$$

are obtained in terms of the torsional angle and of the elements d_η and e_η of the methyl group. The subindex η stands for r, α, or β, depending on the internal valence coordinates involved in each particular symmetry coordinate.

It can be verified that at staggered configurations [$\gamma=(2n+1)\pi/6$, with $n=0,1,2,...$], the symmetry properties of the Raman tensors are those of the degenerate species in D_{3d} point group. At the eclipsed configurations ($\gamma=2n\pi/6$, with $n=0,1,2,...$), the symmetry is as in D_{3h} point group.

2. Raman tensors in normal coordinates representation

Symmetry coordinates S_i and dimensionless normal coordinates q_j are related by

$$S_{i\rho}=L_{ij}q_{j\rho}, \tag{18}$$

where L_{ij} are elements of the vibrational eigenvector L matrix. Consequently, the derivatives of the molecular polarizability are related in the form

$$\frac{\partial\alpha}{\partial q_{i\rho}}=L_{ji}\frac{\partial\alpha}{\partial S_{j\rho}}. \tag{19}$$

For the degenerate coordinates of C_2H_6 indices i and j run from 7 to 12. Index $\rho=a,b$ stands for the two components of a degenerate pair.

Bunker[29,36] has discussed the vibrational GF problem for ethanelike molecules. According to his description, symmetry coordinates, L matrix, and normal coordinates of non-rigid ethane, depend on the torsional angle. In particular, the L matrix consists of four (3×3) blocks of A_{1s} or A_{3s} symmetry expressable as Fourier series in the form

$$\begin{pmatrix} S_{7\rho(E_{1d})} \\ S_{8\rho(E_{1d})} \\ S_{9\rho(E_{1d})} \\ S_{10\rho(E_{2d})} \\ S_{11\rho(E_{2d})} \\ S_{12\rho(E_{2d})} \end{pmatrix} = \begin{pmatrix} ((3\times3)A_{1s}) & ((3\times3)A_{3s}) \\ L_{ij}+\sum_n l_{ij}^{(n)}\cos 6n\gamma & \sum_n l_{ij}^{(n)}\sin 6n\gamma \\ ((3\times3)A_{3s}) & (3\times3)A_{1s}) \\ \sum_n l_{ij}^{(n)}\sin 6n\gamma & L_{ij}+\sum_n l_{ij}^{(n)}\cos 6n\gamma \end{pmatrix} \begin{pmatrix} q_{7\rho(E_{1d})} \\ q_{8\rho(E_{1d})} \\ q_{9\rho(E_{1d})} \\ q_{10\rho(E_{2d})} \\ q_{11\rho(E_{2d})} \\ q_{12\rho(E_{2d})} \end{pmatrix}. \tag{20}$$

The constant terms L_{ij} are known from *ab initio* calculations and empirical force fields[38] with a reasonably degree of confidence. On the contrary, the terms $l_{ij}^{(n)}$ are not known so far. In ethane they are expected to be one order of magnitude smaller than the corresponding L_{ij}'s, or even smaller, by virtue of the relatively high torsional barrier. Setting Eqs. (16) and (17) into Eq. (19), and taking into account Eq. (20), the following nonzero Cartesian components of the γ-dependent Raman tensors are obtained:

(i) E_{1d} normal modes $q_{i\rho}=q_{7\rho},q_{8\rho},q_{9\rho}$, with $\rho=a,b$

$$\frac{\partial\alpha_{xx}}{\partial q_{ia}}=-\frac{\partial\alpha_{yy}}{\partial q_{ia}}=-\frac{\partial\alpha_{xy}}{\partial q_{ib}}=M_i\cos 3\gamma+\sum_n f_i^{(n)}\cos(6n+3)\gamma, \tag{21}$$

$$\frac{\partial\alpha_{yz}}{\partial q_{ia}}=-\frac{\partial\alpha_{xz}}{\partial q_{ib}}=\sum_n g_i^{(n)}\sin 6n\gamma, \tag{22}$$

with

$$M_i=\sqrt{2}(L_{7i}d_r+L_{8i}d_\alpha+L_{9i}d_\beta). \tag{23}$$

(ii) E_{2d} normal modes $q_{i\rho}=q_{10\rho},q_{11\rho},q_{12\rho}$, with $\rho=a,b$

$$\frac{\partial\alpha_{xx}}{\partial q_{ia}}=-\frac{\partial\alpha_{yy}}{\partial q_{ia}}=-\frac{\partial\alpha_{xy}}{\partial q_{ib}}=N_i\sin 3\gamma+\sum_n f_i^{(n)}\sin(6n+3)\gamma, \tag{24}$$

$$\frac{\partial\alpha_{yz}}{\partial q_{ia}}=-\frac{\partial\alpha_{xz}}{\partial q_{ib}}=P_i+\sum_n g_i^{(n)}\cos 6n\gamma, \tag{25}$$

with

$$N_i=\sqrt{2}(L_{10i}d_r+L_{11i}d_\alpha+L_{12i}d_\beta), \tag{26}$$

$$P_i=\sqrt{2}(L_{10i}e_r+L_{11i}e_\alpha+L_{12i}e_\beta), \tag{27}$$

determined by the constant terms of the L matrix and the polarizability parameters of the methyl group. As can be checked from the definition of the irreducible components of the polarizability in Eq. (3), the resulting torsional dependence of the Raman tensors is consistent with that predicted on the sole basis of symmetry (Table II).

In Eqs. (21) to (25), the coefficients $f_i^{(n)}$ and $g_i^{(n)}$ depend on the elements $l_{ij}^{(n)}$ of the γ-dependent L-matrix [Eq. (20)]. In C_2H_6 they are expected to be much smaller than the terms M_i, N_i, and P_i, and will be neglected in the forthcoming discussion. The following derivatives of the irreducible components are then obtained:

(iii) E_{1d} normal modes $q_{i\rho}=q_{7\rho}$, $q_{8\rho}$, $q_{9\rho}$, with $\rho=a,b$

$$\left(\frac{\partial\alpha_{\pm1}^{(2)}}{\partial q_{i\rho}}\right)_\gamma\simeq 0, \tag{28}$$

$$\left(\frac{\partial\alpha_{\pm2}^{(2)}}{\partial q_{ia}}\right)_\gamma=\pm i\left(\frac{\partial\alpha_{\pm2}^{(2)}}{\partial q_{ib}}\right)_\gamma\simeq M_i\cos 3\gamma. \tag{29}$$

(iv) E_{2d} normal modes $q_{i\rho}=q_{10\rho}$, $q_{11\rho}$, $q_{12\rho}$, with $\rho=a,b$

$$i\left(\frac{\partial\alpha_{\pm1}^{(2)}}{\partial q_{ia}}\right)_\gamma=\pm\left(\frac{\partial\alpha_{\pm1}^{(2)}}{\partial q_{ib}}\right)_\gamma\simeq P_i, \tag{30}$$

$$\left(\frac{\partial\alpha_{\pm2}^{(2)}}{\partial q_{ia}}\right)_\gamma=\pm i\left(\frac{\partial\alpha_{\pm2}^{(2)}}{\partial q_{ib}}\right)_\gamma\simeq N_i\sin 3\gamma. \tag{31}$$

Due to the torsional dependence of the quantities of Eqs. (28)–(31), the transition moments $\langle v_4\sigma|\cos 6\gamma|v_4'\sigma'\rangle$, $\langle v_4\sigma|\sin 6\gamma|v_4'\sigma'\rangle$, $\langle v_4\sigma|\cos 3\gamma|v_4'\sigma'\rangle$, and $\langle v_4\sigma|\sin 3\gamma|v_4'\sigma'\rangle$, are also needed for the interpretation of the Raman intensities. A summary of those relevant for the analysis of the spectra discussed below is given in Table V.

TABLE V. Transition moments $\langle v_4\sigma|f(\gamma)|v_4'\sigma'\rangle$ of C_2H_6. Average value over the various torsional symmetries (σ,σ'), with the largest deviation from average value indicated in parenthesis.

$\langle v_4\sigma\|f(\gamma)\|v_4'\sigma'\rangle$	(σ,σ')
$\langle 0\sigma\|\cos 6\gamma\|0\sigma\rangle = -0.847\ 5(0)$	(A_{1s},A_{1s}), (E_{3d},E_{3d}), (E_{3s},E_{3s}), (A_{3d},A_{3d})
$\langle 1\sigma\|\cos 6\gamma\|1\sigma\rangle = -0.537\ 4(16)$	(A_{1d},A_{1d}), (E_{3s},E_{3s}), (E_{3d},E_{3d}), (A_{3s},A_{3s})
$\langle 2\sigma\|\cos 6\gamma\|2\sigma\rangle = -0.209\ 7(218)$	(A_{1s},A_{1s}), (E_{3d},E_{3d}), (E_{3s},E_{3s}), (A_{3d},A_{3d})
$\|\langle 0\sigma\|\cos 6\gamma\|2\sigma\rangle\| = 0.198\ 9(9)$	(A_{1s},A_{1s}), (E_{3d},E_{3d}), (E_{3s},E_{3s}), (A_{3d},A_{3d})
$\|\langle 0\sigma\|\sin 3\gamma\|0\sigma'\rangle\| = 0.959\ 4(0)$	(A_{1s},A_{3d}), (E_{3d},E_{3s})
$\|\langle 1\sigma\|\sin 3\gamma\|1\sigma'\rangle\| = 0.870\ 1(0)$	(A_{1d},A_{3s}), (E_{3s},E_{3d})
$\|\langle 2\sigma\|\sin 3\gamma\|2\sigma'\rangle\| = 0.756\ 3(4)$	(A_{1s},A_{3d}), (E_{3d},E_{3s})
$\|\langle 0\sigma\|\sin 3\gamma\|2\sigma'\rangle\| = 0.057\ 3(1)$	(A_{1s},A_{3d}), (E_{3d},E_{3s}), (E_{3s},E_{3d}), (A_{3d},A_{1s})
$\|\langle 0\sigma\|\sin 3\gamma\|1\sigma'\rangle\| = 0.000\ 2(0)$	(E_{3s},E_{3d}), (E_{3d},E_{3s})
$\|\langle 1\sigma\|\sin 3\gamma\|2\sigma'\rangle\| = 0.005\ 6(0)$	(E_{3s},E_{3d}), (E_{3d},E_{3s})
$\|\langle 2\sigma\|\sin 3\gamma\|3\sigma'\rangle\| = 0.069\ 5(0)$	(E_{3s},E_{3d}), (E_{3d},E_{3s})
$\|\langle 0\sigma\|\cos 3\gamma\|1\sigma'\rangle\| = 0.275\ 6(0)$	(A_{1s},A_{1d}), (E_{3d},E_{3s}), (E_{3s},E_{3d}), (A_{3d},A_{3s})
$\|\langle 1\sigma\|\cos 3\gamma\|2\sigma'\rangle\| = 0.391\ 6(1)$	(A_{1d},A_{1s}), (E_{3s},E_{3d}), (E_{3d},E_{3s}), (A_{3s},A_{3d})
$\|\langle 2\sigma\|\cos 3\gamma\|3\sigma'\rangle\| = 0.482\ 6(80)$	(A_{1s},A_{1d}), (E_{3d},E_{3s}), (E_{3s},E_{3d}), (A_{3d},A_{3s})
$\|\langle 0\sigma\|\cos 3\gamma\|0\sigma'\rangle\| = 0.000\ 03(0)$	(E_{3s},E_{3d})
$\|\langle 1\sigma\|\cos 3\gamma\|1\sigma'\rangle\| = 0.001\ 4(0)$	(E_{3s},E_{3d})
$\|\langle 2\sigma\|\cos 3\gamma\|2\sigma'\rangle\| = 0.023\ 6(0)$	(E_{3s},E_{3d})
$\|\langle 0\sigma\|\sin 6\gamma\|1\sigma'\rangle\| = 0.483\ 3(3)$	(A_{1s},A_{3s}), (E_{3d},E_{3d}), (E_{3s},E_{3s}), (A_{3d},A_{1d})
$\|\langle 1\sigma\|\sin 6\gamma\|2\sigma'\rangle\| = 0.576\ 0(56)$	(A_{1d},A_{3d}), (E_{3s},E_{3s}), (E_{3d},E_{3d}), (A_{3s},A_{1s})
$\|\langle 2\sigma\|\sin 6\gamma\|3\sigma'\rangle\| = 0.544\ 9(375)$	(A_{1s},A_{3s}), (E_{3d},E_{3d}), (E_{3s},E_{3s}), (A_{3d},A_{1d})

They have been calculated from the torsional wave functions $|v_4\sigma\rangle$, obtained by numerical diagonalization of the torsional Hamiltonian

$$H_T = -A\frac{\partial^2}{\partial\gamma^2} + \frac{V_3}{2}(1+\cos 6\gamma) + \frac{V_6}{2}(1-\cos 12\gamma), \tag{32}$$

in the basis of the free rotor functions $|L\rangle = \mathscr{N}^{-1}\exp(iL\gamma)$, following the procedure of Ref. 17.

At this point it is worth discussing the symmetry properties of the torsional-dependent Raman tensors, in order to trace the conceptual transition from D_{3d} to G_{36}^+. Raman active degenerate vibrations of C_2H_6, and the polarizability components $\alpha_{\pm1}^{(2)}$ and $\alpha_{\pm2}^{(2)}$, belong to the E_g species in D_{3d},[27] so that two series of transitions $\Delta k = \pm 1$ and $\Delta k = \pm 2$ are expected in the spectrum, each series with an intensity given by an independent component $(\partial\alpha_{\pm1}^{(2)}/\partial q)^2$ and $(\partial\alpha_{\pm2}^{(2)}/\partial q)^2$, whose ratio is constant for a given band. On the contrary, $\alpha_{\pm1}^{(2)}$ and $\alpha_{\pm2}^{(2)}$ transform like different degenerate representations (E_{2d} and E_{1s}) in G_{36}^+,[27] so that the selection rules for a given degenerate vibrational band of ethane are apparently $\Delta k = \pm 1$ or $\Delta k = \pm 2$, *but not both*, depending on whether the vibration belongs to the E_{2d} or E_{1s} species of G_{36}^+. As a matter of fact, the analysis of ν_{10} and ν_{11} by Lepard *et al.*[12] showed that both series of sub-branches $\Delta k = \pm 1$ and $\Delta k = \pm 2$ were present in the spectrum of these two bands.

This apparent contradiction is overcome when the torsional dependence of the Raman tensors is taken into account. For a (E_{1d},E_{2d}) pair of normal modes, several conclusions can be drawn from Eqs. (28) to (31). First, the only constant term (i.e., independent from γ) is that of $\alpha_{\pm1}^{(2)}$ of the E_{2d} symmetry. This is the meaning to be attributed to the notation in the Character Table of G_{36}^+, as given in Ref. 27. The $\Delta k = \pm 2$ transitions, that seemed to be "lost" in going from the D_{3d} to G_{36}^+ descriptions of ethane, become allowed by means of the term in $\sin 3\gamma$. And the E_{1d} modes, which, according to the Character Table of G_{36}^+, were active in IR but not in Raman, become allowed in Raman with rotational selection rules $\Delta k = \pm 1$ and $\Delta k = \pm 2$, through the terms in $\sin 6\gamma$ and $\cos 3\gamma$. The terms in γ mean that these transitions involve a simultaneous change in the torsional state, but because of the different symmetry of the γ functions, these torsional transitions are different for the E_{2d} modes than for the E_{1d}, as can be checked with the transition moments in Table V: in the E_{2d} case, they imply $\Delta v_4 = 0$, but connect $A_{1s}\leftrightarrow A_{3d}$, $A_{3s}\leftrightarrow A_{1d}$, and $E_{3s}\leftrightarrow E_{3d}$, i.e., there is a change in the torsional wave function but *within* the same torsional quantum number v_4; on the contrary, in the E_{1d} case, they necessarily convey a $\Delta v_4 = \pm 1$ change, thus becoming allowed in the form of a torsional combination or difference band, $(\nu \pm \nu_4)$, as expected in the D_{3d} description.

Furthermore, according to the model for the torsional dependence of the Raman tensors just described, the intensity of the $\alpha_{\pm2}^{(2)}$ component of an E_g mode in D_{3d} is "split" into the E_{1d} (IR) and the E_{2d} (Raman) modes in G_{36}^+. Thus, we can look at this situation in terms of the IR modes "borrowing" some intensity from the Raman ones when the torsional motion departs from a small amplitude vibration. This poses a relation between the intensity of a Raman degenerate vibrational band and the combination or difference of its IR counterpart with the torsional mode, that can be used to check the applicability of the model.

III. EXPERIMENTAL RESULTS AND DISCUSSION

A. Instrumentation

The Raman spectra shown below have been recorded with a high-sensitivity instrument.[39] It is equipped with a low noise CCD detector (512×512 pixels, 19×19 μm^2 pixel size) refrigerated by liquid N_2, and a computer controlled scanning/data acquisition system which allows spectral accu-

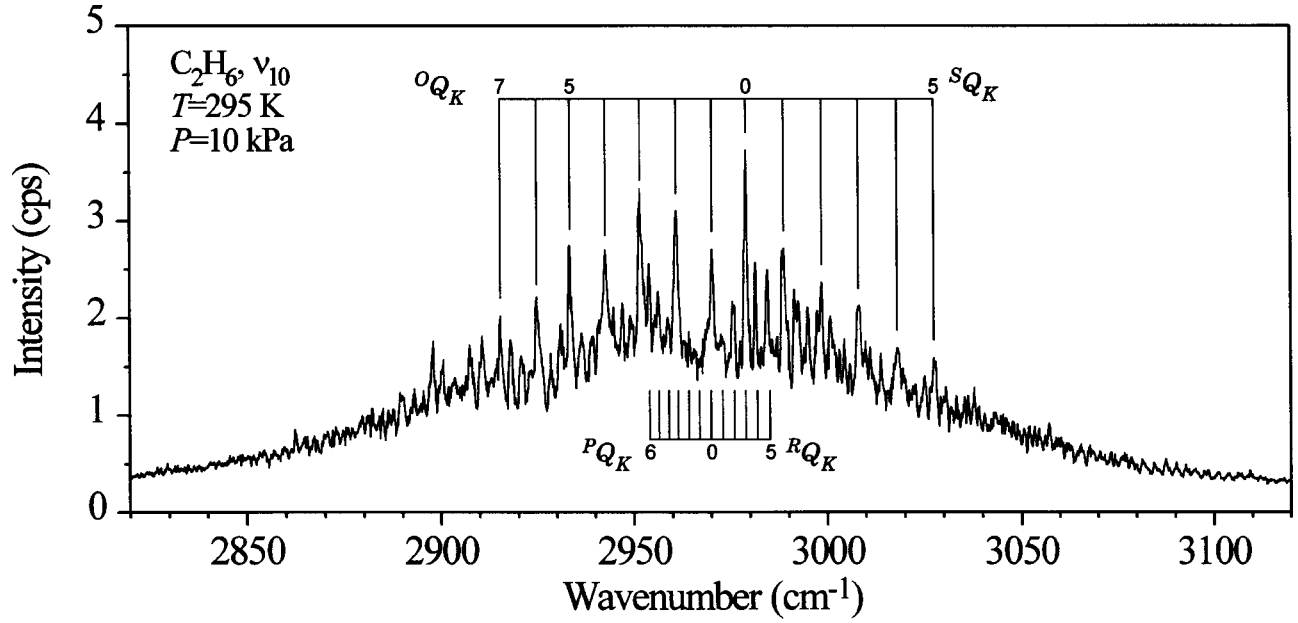

FIG. 4. The ν_{10} Raman band of gaseous ethane. $[YX]$ scattering geometry excited with 1.0 W (+multipass) at 514.5 nm. Average of 10 scans in ~3 h total acquisition time, using 50 μm≡0.40 cm^{-1} spectral slit. CCD binning: 1×256 pixels.

mulation without loss of resolution. The detection threshold is about 1 ppm, referred to a gas at standard temperature and pressure, using 1 W exciting *cw*-laser power at 514.5 nm. The spectral resolution of the instrument is on the order of 0.2 cm^{-1}.

The large sample chamber of 42×42×24 cm^3, manufactured in aluminum, and blackened inside to reduce stray radiation, allows recording two sorts of Raman spectra

(i) from gases under supersonic jet conditions, in the temperature range $5<T<100$ K, and
(ii) from static gases in the pressure range $0.1<P<200$ kPa.

The first sort of spectra can just be recorded for intense Raman bands, due to the signal limitation imposed by the rarefaction proper of supersonic expansions. In the present case, among the degenerate bands of C_2H_6, only ν_{10} and ν_{11} are intense enough to be recorded under expansion conditions in a wide thermal range. In order to extend this range down to the lowest temperatures, besides pure C_2H_6 (Air Liquide, 99.4% stated purity), mixtures of 50%, 20%, and 5% of C_2H_6 in He were expanded through a nozzle of diameter $D=300\ \mu$m, under stagnation temperature of 295 K and pressure of 100 kPa.

The other bands investigated, namely ν_{12}, $\nu_7+\nu_4$, $\nu_8+\nu_4$, $\nu_{11}+\nu_{12}$, and $\nu_8+2\nu_4-\nu_9$, are at least two orders of magnitude weaker than ν_{10}, and were not amenable to observation under supersonic expansion. Their Raman spectra were recorded at a pressure of 10 kPa in order to reduce the pressure broadening.

Wave numbers were calibrated either with emision lines of Ne, or with the $S(1)$ Raman line of O_2 at 1570.53 cm^{-1}.[40] The estimated accuracy is ±0.1 cm^{-1}.

B. $\nu_{10}(E_{2d})$, $\nu_{11}(E_{2d})$, and $\nu_{12}(E_{2d})$ fundamental bands

The Raman spectra of ν_{10} and ν_{11} bands of ethane were investigated in some detail in the prelaser era:[12] they were recorded photographically with an exposure time of about 70 h, at a sample pressure of one atmosphere. In the prelaser spectrum of ν_{10}, a large number of rotation–vibration lines were overlapped by the strong Q branches of ν_u at 2954 cm^{-1}, and of ν_l at 2898 cm^{-1}, of the Fermi resonance of ν_1.[16] The prelaser spectrum of ν_{11} was somewhat better.

In spite of the relatively modest signal-to-noise ratio, and of the low resolution caused by pressure broadening, a rather complete analysis of the spectra of ν_{10} and ν_{11} was accomplished.[12] However, doubts remained about the vibrational origin of both bands, which could be misassigned by ±1 unit of the quantum number k. Further, the ratio of transition moments

$$R_i=\left(\frac{\langle VT|\left(\frac{\partial\alpha^{(2)}_{\pm 2}}{\partial q_{i\rho}}\right)_\gamma q_{i\rho}|V'T'\rangle}{\langle VT|\left(\frac{\partial\alpha^{(2)}_{\pm 1}}{\partial q_{i\rho}}\right)_\gamma q_{i\rho}|V'T'\rangle}\right)^2 =\left(\frac{N_i}{P_i}\right)^2|\langle T|\sin 3\gamma|T'\rangle|^2, \tag{33}$$

(referred to in Ref. 12 as $C_{\pm 2}:C_{\pm 1}$) was defined in the frame of a D_{3d} point group, i.e., ommitting the angular dependence in γ; prelaser values of R_i were not expected to be determined accurately neither for ν_{10}, nor for ν_{11}, due to the low signal-to-noise ratio of the photographically recorded spectra.

We report here the ν_{10} and ν_{11} bands recorded with improved experimental conditions: at room temperature and

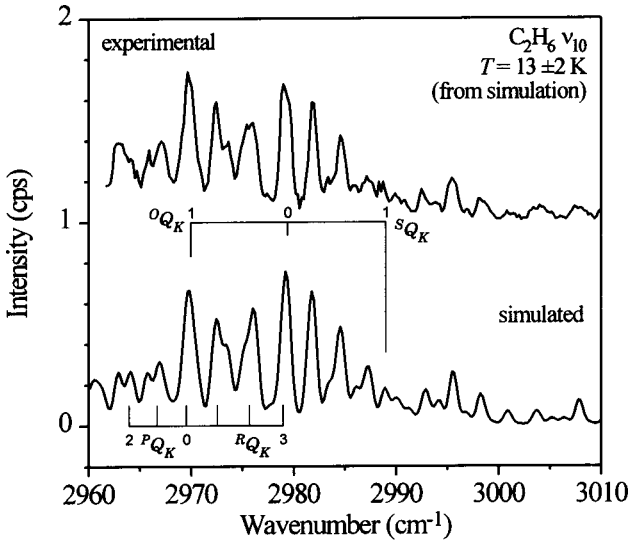

FIG. 5. The ν_{10} Raman band of jet-expanded ethane (5% in He), at $x=5D=1.5$ mm from nozzle and 10^5 Pa stagnation pressure. $[YY]+[YX]$ scattering geometry excited with 2.0 W at 514.5 nm. Average of 2 scans in 10 min total acquisition time, using 100 μm$\equiv$0.80 cm^{-1} spectral slit. CCD binning: 3×256 pixels.

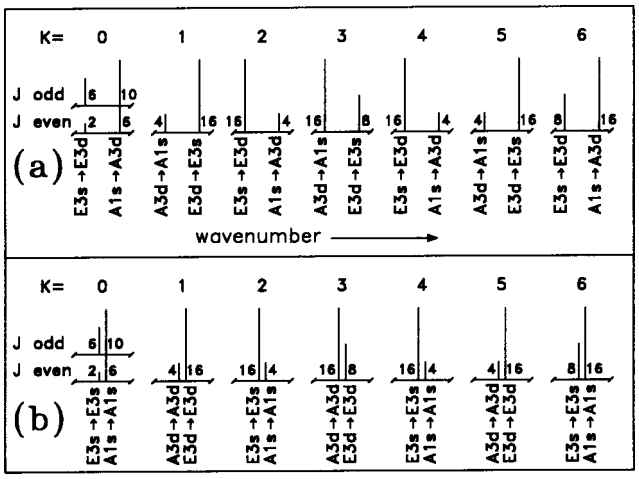

FIG. 6. High resolution torsional splitting patterns for torsional–rotational Raman transitions from ground to an $\Gamma_{vib}=E_{2d}$ degenerate vibrational state. (a) $\Delta k=\pm2$; (b) $\Delta k=\pm1$. For each transition, symmetries of initial and final torsional wave functions, rotational quantum number k (mod 6) of initial state, and relative intensity due to nuclear spin weight are given.

pressure of 10 kPa, and under supersonic expansion, at temperatures ranging from ~100 K down to 13 K. The low temperature spectra were aimed to remove any ambiguity about the band origin.

Some representative spectra of ν_{10} are shown in Fig. 4 (room temperature) and Fig. 5 (13 K). The spectrum in Fig. 4 was recorded under 90° scattering geometry $X[YX]Z$ in order to avoid the overlapping of the much more intense nondegenerate bands. It can be noticed in Fig. 4 the complete elimination of the strongly polarized components $\nu_u=2954\,\mathrm{cm}^{-1}$ and $\nu_l=2898\,\mathrm{cm}^{-1}$ of the Fermi resonance involving ν_1. Some assignments of prominent peaks are indicated in Figs. 4 and 5, calculated from the analysis described next.

TABLE VI. Molecular constants of selected vibrational states of $^{12}C_2H_6$.

State	Ref.	state	Ref.
$\nu_7(E_{1d})=2985.39\ \mathrm{cm}^{-1}$	9	$\nu_{10}(E_{2d})=2968.48\pm0.1\ \mathrm{cm}^{-1}$	a
$A_7=2.682\ \mathrm{cm}^{-1}$	9	$A_{10}=2.712\,8\pm0.002\ \mathrm{cm}^{-1}$	a
$B_7=0.663\,10\ \mathrm{cm}^{-1}$	9	$B_{10}=0.664\,7\pm0.000\,3\ \mathrm{cm}^{-1}$	a
$\zeta_7^z=0.128$	9	$\zeta_{10}^z=0.219\pm0.002$	a
		$R_{10}=0.6\pm0.2$	a
$\nu_8(E_{1d})=1471.634\ \mathrm{cm}^{-1}$	6	$\nu_{11}(E_{2d})=1468.4\pm0.1\ \mathrm{cm}^{-1}$	a
$A_8=2.656\,02\ \mathrm{cm}^{-1}$	6	$A_{11}=2.657\,5\pm0.001\ \mathrm{cm}^{-1}$	a
$B_8=0.664\,667\ \mathrm{cm}^{-1}$	6	$B_{11}=0.666\,6\pm0.000\,5\ \mathrm{cm}^{-1}$	a
$\zeta_8^z=-0.302\,5$	6	$\zeta_{11}^z=-0.334\,39$	18
		$R_{11}=0.35\pm0.15$	a
$\nu_9(E_{1d})=821.722\,44\ \mathrm{cm}^{-1}$	2	$\nu_{12}(E_{2d})=1196.9\pm0.2\ \mathrm{cm}^{-1}$	a
$A_9=2.678\,900\,8\ \mathrm{cm}^{-1}$	2	$A_{12}=(2.669\,52)\ \mathrm{cm}^{-1}$	b
$B_9=0.661\,744\,3\ \mathrm{cm}^{-1}$	2	$B_{12}=(0.663\,027\,4)\ \mathrm{cm}^{-1}$	b
$\zeta_9^z=0.259\,334\,7$	2	$\zeta_{12}^z=0.407\pm0.01$	a
		$R_{12}\geqslant3$	a
Ground state		Torsion	
$A_0=2.669\,52\ \mathrm{cm}^{-1}$	37	$\nu_4=289\ \mathrm{cm}^{-1}$	17
$B_0=0.663\,027\,4\ \mathrm{cm}^{-1}$	33	$A_4=2.674\,5\ \mathrm{cm}^{-1}$	41
$D_J=1.031\,74\times10^{-6}\ \mathrm{cm}^{-1}$	2	$B_4=0.660\,501\,1\ \mathrm{cm}^{-1}$	33
$D_{Jk}=2.660\,4\times10^{-6}\ \mathrm{cm}^{-1}$	2		
$D_k=9.44\times10^{-6}\ \mathrm{cm}^{-1}$	38		

[a]Present work.
[b]Ground state value.

The Raman spectra of ν_{10} in Figs. 4 and 5, plus other at intermediate temperatures (46 and 79 K), were simulated using Eq. (2) for the intensities, and the expresion

$$E_{VR}(\nu^l Jk)=\omega v+B_v J(J+1)+(A_v-B_v)k^2+A_v(\zeta_v^z l)^2-2A_v\zeta_v^z kl-D_J(J(J+1))^2-D_{Jk}J(J+1)k^2-D_K k^4, \quad (34)$$

for the energies of the rotation–vibration levels. This simulation allowed some molecular constants of the band to be fitted to the experimental spectrum. The results are shown in Table VI.

As shown in Fig. 5, a reasonably good simulation of the spectrum of ν_{10} at a temperature of $T=13$ K is possible on the basis of the parameters of Table VI. At temperatures above 50 K, the population of levels involving higher J values becomes dominant and the simulation becomes poorer, with evidence of local perturbations. Nonetheless, it was possible to obtain the A_{10}, B_{10}, and ζ_{10}^z constants from fits of the low temperature spectra, and to confirm unambiguously the band origin. Our analysis, summarized in Table VI (rows for ν_{10}) largely confirms that of Lepard *et al.*[12]

From the ratio $R_{10}=0.6\pm0.2$, defined in Eq. (33), jointly with the absolute cross section[13] of ν_{10}, one obtains the numerical values of the main coefficients of the Raman tensors defined in Eqs. (24) and (25)

$$|N_{10}|=(0.166\pm0.017)\times10^{-40}\ \mathrm{C\,m^2\,V^{-1}},$$
$$|P_{10}|=(0.198\pm0.02)\times10^{-40}\ \mathrm{C\,m^2\,V^{-1}}. \quad (35)$$

The ν_{10}, ν_{11}, and ν_{12} bands obey the selection rules number 9 and 13 of Table III, shown in detail in Fig 3. The expected torsional splittings cannot be resolved under the present experimental conditions. However, the (unperturbed)

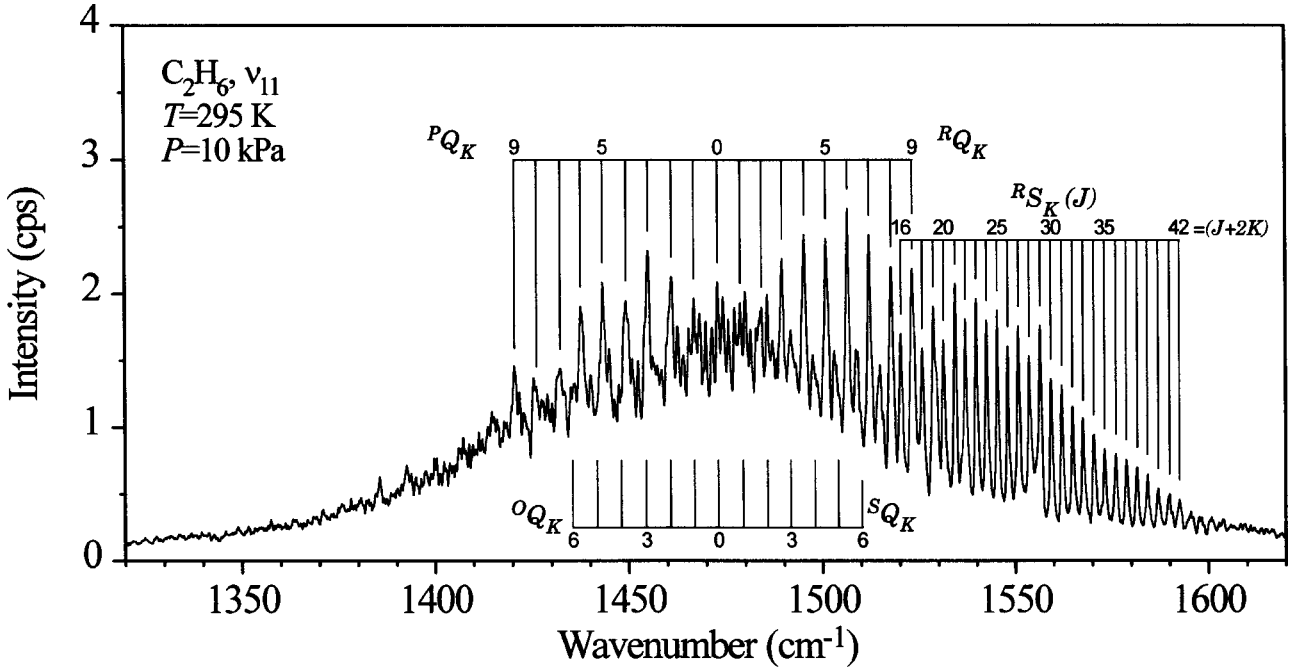

FIG. 7. The ν_{11} Raman band of gaseous ethane. $[YY]+[YX]$ scattering geometry excited with 1.0 W (+multipass) at 514.5 nm. Average of 10 scans in ~2.5 h total acquisition time, using 50 μm≡0.52 cm^{-1} spectral slit. CCD binning: 1×256 pixels.

high resolution pattern can be predicted with the aid of Figs. 2 and 3. As shown in Fig. 6(a), the transitions J, $k \rightarrow J'$, $k \pm 2$ are expected to consist of torsional doublets separated by approximately $6X = 0.011\ cm^{-1}$, with the ratio of intensities and the ordering of the splitting components depending on the quantum number k of the initial level of the transition. On the contrary, for J, $k \rightarrow J'$, $k \pm 1$ transitions, the torsional splittings are expected to be much smaller, just due to the difference of the effective torsional barrier between the ground and the vibrational level ν_{10}. Thus, the order shown in Fig. 6(b) is uncertain, and could be globally reversed. Rotational and torsional perturbations can modify this pattern, even lifting the A_1/A_2 or E_3/E_4 degeneracies in Fig. 3. In particular, the Coriolis perturbation of ν_{10} by the nearby ν_1 fundamental can be expected through the $\zeta^{xy}_{1,10}$ term.

The Raman spectra of ν_{11} are shown in Fig. 7 (room temperature) and Fig. 8 (23 K). These and other spectra at intermediate temperatures were analyzed in a similar way to ν_{10}, just discussed. The results are included in Table VI. From the fits it was possible to determine the band origin and the rotational constants A_{11} and B_{11}; ζ^z_{11} was fixed at the value from the analysis of the IR combination[18] $\nu_{11}+\nu_4$. From $R_{11}=0.34\pm0.15$, jointly with the absolute cross section[13] of ν_{11}, one obtains

$$|N_{11}| = (0.060 \pm 0.01) \times 10^{-40}\ \mathrm{C\,m^2\,V^{-1}},$$
$$|P_{11}| = (0.097 \pm 0.015) \times 10^{-40}\ \mathrm{C\,m^2\,V^{-1}}. \quad (36)$$

Some assignments of prominent peaks, calculated from the molecular constants of Table VI are indicated in Figs. 7 and 8: positions of Q_K sub-branches and the result of accidental piling up of ${}^RS_K(J)$ transitions with the same value of $(J+2K)$. Due to the negative sign of the Coriolis ζ^z_{11} constant, it should be noticed that the order of the $+l$ and $-l$ components of the energy levels of ν_{11} is reversed with respect to Figs. 2 and 3.

The Raman spectrum in the region of the ν_{12} band is shown in Fig. 9. For the ν_{12} band, barely investigated before, present analysis provides strong evidence that its previous assignment[13,15] was not correct. As shown in Fig. 9, the broad peak at $\nu \simeq 1190\ cm^{-1}$ previously assigned as ν_{12}, turns out to be completely polarized. Thus, it cannot be assigned to a degenerate fundamental band. It may be better assigned to the difference band $(\nu_8+2\nu_4)-\nu_9$, analyzed

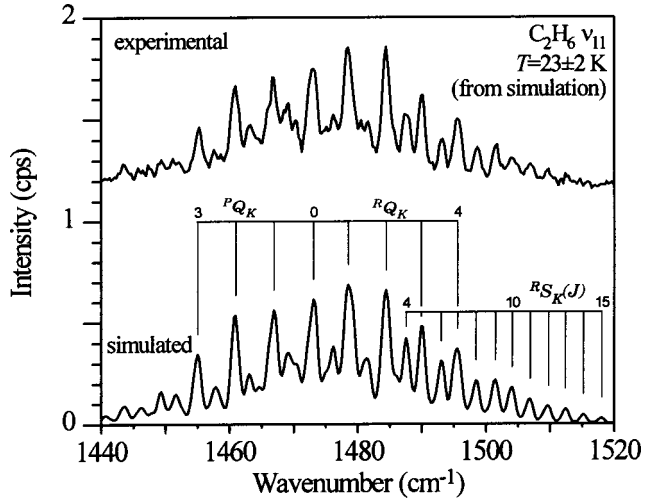

FIG. 8. The ν_{11} Raman band of jet-expanded ethane (20% in He), at $5D = 1.5$ mm from nozzle and 1 bar stagnation pressure. $[YY]+[YX]$ scattering geometry, excited with 1.5 W (+multipass) at 514.5 nm. Average of 5 scans in 25 min total acquisition time, using 100 μm≡1.03 cm^{-1} spectral slit. CCD binning: 3×256 pixels.

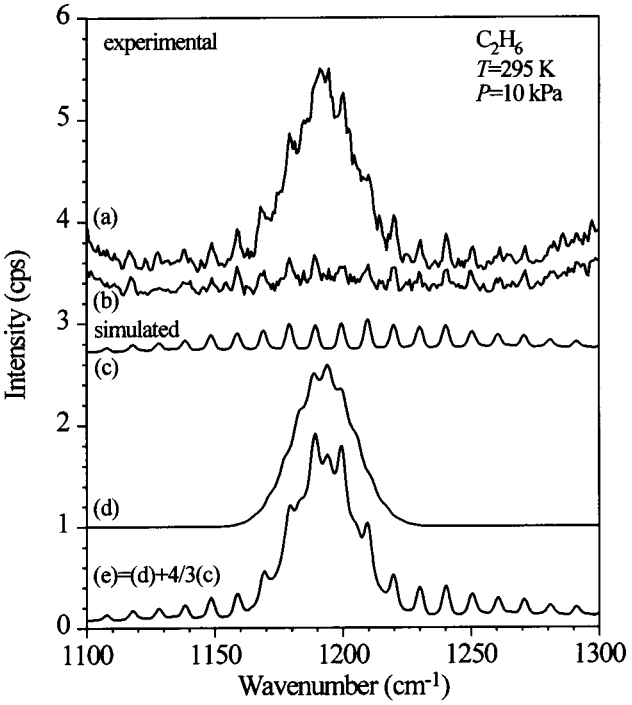

FIG. 9. Raman spectrum of gaseous ethane in the region of the ν_{12} band. (a) and (b) experimental, excited with 2 W (+multipass) at 514.5 nm, using 300 μm≡3.2 cm^{-1} spectral slit; scattering geometry: (a) $[YY]$; (b) $[YX]$, total acquisition time: 30 min each, CCD binning: 8×256 pixels. (c) simulated ν_{12} band with $R_{12}=\infty$. (d) simulated $(\nu_8+2\nu_4)-\nu_9$ band. (e) sum of 4/3(c) +(d).

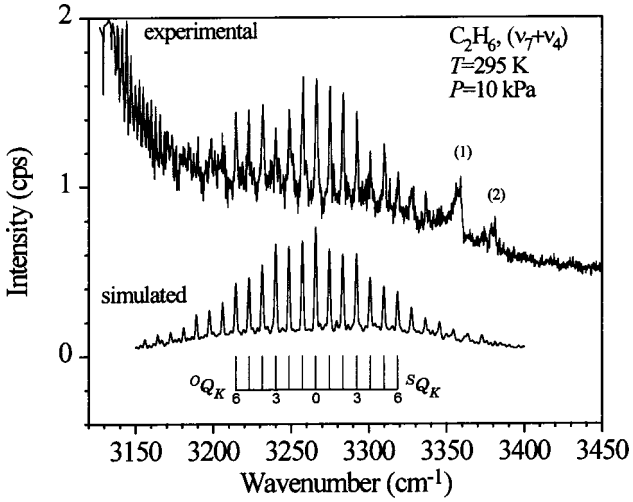

FIG. 10. Raman spectrum of gaseous ethane in the region of the $\nu_7+\nu_4$ band. $[YY]+[YX]$ scattering geometry excited with 2 W+multipass at 514.5 nm. Average of 9 scans in ~4 h total acquisition time, using 100 μm≡0.76 cm^{-1} spectral slit. CCD binning: 3×256 pixels. (1) and (2) tentatively assigned as $2\nu_2+2\nu_4$ and $\nu_3+2\nu_{12}$, respectively.

below in some detail. The actual ν_{12} band is the broad underlying structure seen in Fig. 9(b) with average spacing of $\Delta=10.22$ cm^{-1} between consecutive peaks. This spacing is consistent with that of the ^OQ_K and ^SQ_K sub-branches for a Coriolis constant of 0.40, close to the value $\zeta^z_{12}=0.4063$ derived[6] from the analysis of the IR spectrum of $\nu_{12}+\nu_4$. From the fit to the experimental spectrum shown in Fig. 9(b) the ζ^z_{12} constant and the band origin were obtained, as reported in Table VI. However, due to the extremely low intensity of ν_{12}, and the overlapping of the broad feature centered at ~1190 cm^{-1}, it is not possible from present spectra to determine unambiguously the band origin. We propose

$$\nu_{12}=1196.9\pm0.2\,\mathrm{cm}^{-1}(\pm n\times\Delta), \tag{37}$$

with $n=0$, or 1, or 2.

The cross section of ν_{12} is estimated to be about one fourth of the very small value reported earlier.[13] This imposes onto $|N_{12}|$ and $|P_{12}|$ the constraint

$$0.857|N_{12}|^2+|P_{12}|^2\leqslant 0.000\,171\times10^{-80}\ \ \mathrm{C}^2\,\mathrm{m}^4\,\mathrm{V}^{-2}. \tag{38}$$

With the aid of Eqs. (26)–(27), and of the L matrix of the vibrational force field of ethane,[38] the quantities $|N_i|$ and $|P_i|$, for $i=10$, 11, 12, can be reduced to the parameters d_r, e_r, d_α, e_α, d_β, and e_β of the methyl group tensors, defined in Eqs. (14), (15), and analogous ones. The parameters obtained are $|d_r|=1.07\pm0.1$, $|e_r|=1.27\pm0.1$, $|d_\alpha|\leqslant0.25$, $|e_\alpha|\leqslant0.30$, $|d_\beta|\leqslant0.14$, $|e_\beta|\leqslant0.16$, in units of $10^{-30}\,\mathrm{C\,m\,V}^{-1}$. The following values have been derived from *ab initio* calculations:[26] $d_r=0.717$, $e_r=0.742$, $d_\alpha=-0.129$, $e_\alpha=0.181$, $d_\beta=-0.055$, and $e_\beta=0.116$, in the same units. From this analysis, it turns out that over 90% of the Raman intensity of the ν_{11} band arises from the C–H stretching coordinate S_{10} in the q_{11} normal mode.

C. $\nu_7(E_{1d})+\nu_4$, $\nu_8(E_{1d})+\nu_4$, and $\nu_9(E_{1d})+\nu_4$ vibration–torsion combination bands

The theoretical model described in Sec. II provides selection rules and Raman tensors for transitions to any degenerate vibrational state in C_2H_6 involving an arbitrary number of torsional quanta. These Raman tensors are also determined by the six quantities d_r, e_r, d_α, e_α, d_β, e_β of the methyl group, defined in Eqs. (14) and (15), whose numerical values were given above.

The Raman tensors for the normal coordinates q_7, q_8, and q_9 of E_{1d} vibrational symmetry are largely determined by the quantities M_7, M_8, and M_9, respectively, defined in Eq. (23). Their numerical values are $|M_7|=0.166\pm0.017$, $|M_8|=0.073\pm0.014$, and $|M_9|\leqslant0.024$, in units of $10^{-40}\,\mathrm{C\,m^2\,V^{-1}}$, as calculated from the L_{ij} coefficients derived from the empirical force field of ethane.[38]

All $\nu_7+\nu_4$, $\nu_8+\nu_4$, and $\nu_9+\nu_4$ combination bands are permitted in the Raman spectrum, and, according to Table III, obey the torsional selection rules No. 3 and 7. However, from Eq. (28), the $\Delta k=\pm1$ transitions should have almost zero intensity. Hence, the ^PQ_K and ^RQ_K peaks should be nearly missing, and only the ^OQ_K and ^SQ_K peak series would be observed. The Raman cross section associated with the $\Delta k=\pm2$ transitions is determined by the quantities M_7, M_8, and M_9 given above, along with the square of the torsional transition moment $\langle0\sigma|\cos3\gamma|1\sigma'\rangle$ given in Table V.

On this basis, we obtain for $\nu_7(E_{1d})+\nu_4$ a cross section that is 0.035 of the nearby $\nu_{10}(E_{2d})$ band. In Fig. 10, the Raman spectrum of ethane in the region 3100–3450 cm^{-1} is shown. The dominant feature is a series of sharp peaks with an average spacing of $\Delta=8.74$ cm^{-1}. This spacing matches well with the spacing $\Delta=8.71$ calculated for $\nu_7+\nu_4$ from[9]

$\zeta_7^z = 0.128$. In Fig. 10, the simulated spectrum of $\nu_7 + \nu_4$, resulting from a fit to the experimental spectrum, is also shown. The following molecular constants for $\nu_7 + \nu_4$ are determined from the fit:

$$\nu_7 + \nu_4 = 3256.55 \pm 0.04 \ \text{cm}^{-1}, \tag{39}$$

$$\zeta^z(\nu_7 + \nu_4) = 0.112 \pm 0.003, \tag{40}$$

$$A(\nu_7 + \nu_4) - A_0 = 0.017 \pm 0.003 \ \text{cm}^{-1}. \tag{41}$$

This origin is, however, uncertain by $\pm\Delta$ or $\pm 2\Delta$, due to the low signal to noise ratio of the experimental spectrum. We thus conclude that this band may be attributed to $\nu_7(E_{1d}) + \nu_4$, instead of the previously proposed assignment as the ${}^S S_K$ of ν_{10} band,[15] or as the ${}^S S_K$ of ν_1 band.[42] The experimental intensity for $\nu_7(E_{1d}) + \nu_4$ appears to be somewhat weaker than predicted, but the determination of the baseline is uncertain.

By the same token, the counterpart band $\nu_8(E_{1d}) + \nu_4$, with the same symmetry characteristics as $\nu_7(E_{1d}) + \nu_4$, should be expected around 1760 cm^{-1}. However, it should be still weaker than $\nu_7(E_{1d}) + \nu_4$, by about one order of magnitude, since its intensity is given by $(M_8)^2$, which is smaller than $(M_7)^2$. Indeed, such a band has been reported,[15] tentatively assigned as $3\nu_4 + \nu_9$, $2\nu_4 + \nu_{12}$, or $\nu_4 + \nu_8$ (the quotation in the original,[15] $\nu_4 + \nu_9$, is thought to be a misprint). Though the signal-to-noise ratio is not very good, the average spacing between consecutive ${}^{O,S}Q_K$ branches, of about[15] 7 cm^{-1}, is more consistent with the assignment as $\nu_8(E_{1d}) + \nu_4$ band. The $\nu_9(E_{1d}) + \nu_4$ band, with estimated origin at about 1111 cm^{-1}, should be still much weaker then the previous bands due to the very small value of M_9.

The corresponding torsional hot bands, with origins at $\nu_7(E_{1d}) - \nu_4 \simeq 2696$, $\nu_8(E_{1d}) - \nu_4 \simeq 1182$, and $\nu_9(E_{1d}) - \nu_4 \simeq 533\,\text{cm}^{-1}$, should display a similar structure of ${}^{O,S}Q_K$ branches as their counterpart combination bands discussed above, with intensities weaker by a population factor $F = \exp(-hc\nu_4/k_B\Theta) = 0.24$ at room temperature. According to Table III, the selection rules for these bands are 2 and 6.

D. $\nu_{11}(E_{2d}) + \nu_{12}(E_{2d})$ combination band

In Fig. 11, the Raman spectrum of ethane in the region 2500–2750 cm^{-1} is shown. The $\nu_{11}(E_{2d}) + \nu_{12}(E_{2d})$ band, expected in this region, has three components: $(\nu_{11} + \nu_{12})_{A_{1s}}$ and $(\nu_{11} + \nu_{12})_{E_{1s}}$, which are Raman active, and the inactive one $(\nu_{11} + \nu_{12})_{A_{2s}}$. The $(\nu_{11} + \nu_{12})_{A_{1s}}$ component is expected to have a sharp and very weak Q branch[24] that may be tentatively assigned in Fig. 11 as the peak (2) at about 2661 cm^{-1}.

Though Table III refers to selection rules of fundamentals with arbitrary torsional quanta, it also applies to overtones and combinations by replacing the first derivative of the polarizability by the second derivative of the same symmetry, according to Table II. So $(\nu_{11} + \nu_{12})_{E_{1s}}$ obeys selection rules 17 and 21. In principle, one can expect for $(\nu_{11} + \nu_{12})_{E_{1s}}$ a set of ${}^{O,S}Q_K$ branches, its intensity originating from a nearly constant derivative $\partial^2\alpha_{\pm 2}^{(2)}/\partial q_{11}\partial q_{12}$, and another set of ${}^{P,R}Q_K$ branches due to a modulated term $\partial^2\alpha_{\pm 1}^{(2)}/\partial q_{11}\partial q_{12}$ with γ dependence of the form $\sin(6n+3)\gamma$. The observed average spacing of 7.48 cm^{-1} is consistent with the predicted one, $\Delta = 7.64$ cm^{-1}, for the ${}^{O,S}Q_K$ branches for an effective $\zeta^z = -(\zeta_{11}^z + \zeta_{12}^z) = -0.0726$, from the values of Table VI. In Fig. 11, the simulated spectrum of $(\nu_{11} + \nu_{12})_{E_{1s}}$, resulting from a fit to the experimental spectrum, is also shown. The following molecular constants are determined from the fit:

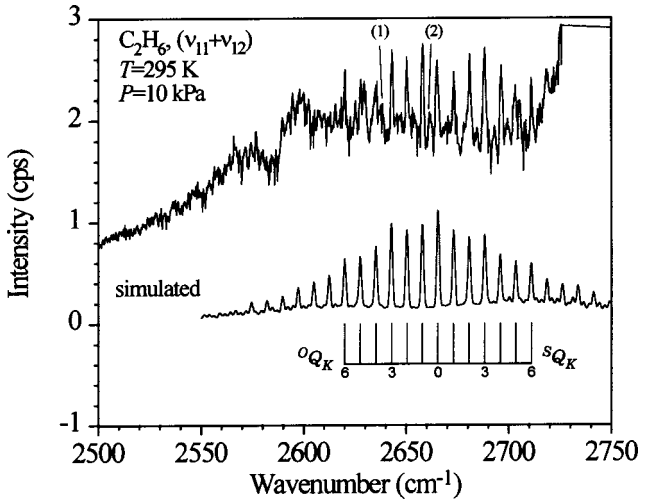

FIG. 11. Raman spectrum of gaseous ethane in the region of the $\nu_{11} + \nu_{12}$ band. $[YY] + [YX]$ scattering geometry excited with 2 W+multipass at 514.5 nm. Average of 10 scans in ~2.5 h total acquisition time, using 100 μm≡0.85 cm^{-1} spectral slit. CCD binning: 3×256 pixels. (1) and (2) tentatively assigned as $\nu_3 + 2\nu_9$ and $(\nu_{11} + \nu_{12})(A_{1s})$, respectively.

$$(\nu_{11} + \nu_{12})_{E_{1s}} = 2658.29 \pm 0.05 \ \text{cm}^{-1}, \tag{42}$$

$$\zeta^z(\nu_{11} + \nu_{12})_{E_{1s}} = -0.081 \pm 0.003. \tag{43}$$

As in the case of $\nu_7 + \nu_4$, the origin of $(\nu_{11} + \nu_{12})_{E_{1s}}$ could be misassigned by $\pm\Delta$ or $\pm 2\Delta$. The previous assignment[15] as the ${}^O O_K$ band of ν_{10} does not appear to be consistent with the present analysis.

E. $\nu_8(E_{1d}) + 2\nu_4 - \nu_9(E_{1d})$ difference band

In Fig. 9 the very weak—and strongly polarized—band centered at ~1190 cm^{-1} is shown. This band, previously assigned[13,15] as ν_{12}, instead seems to correspond to a transition between two vibrational states of symmetry E_{1d}, $\nu_9 \rightarrow (\nu_8 + 2\nu_4)$. If so, it owes its intensity chiefly to the term $\partial\alpha_0^{(0)}/\partial q_8 \partial q_9$, and thus obeys the rotational selection rules $\Delta J = 0$, $\Delta k = 0$, and $\Delta l = 0$, and the torsional rules $A_{1s} \rightarrow A_{1s}$, $E_{3d} \rightarrow E_{3d}$, $E_{3s} \rightarrow E_{3s}$, and $A_{3d} \rightarrow A_{3d}$. The reason why this Q branch is unusually broad is the combined effect of large Coriolis constants, $\zeta_8^z \simeq -0.30$ in the final level and $\zeta_9^z = 0.259\,334$ in the initial level, with opposite signs. This causes a splitting between consecutive ${}^Q Q_K$ branches of about

$$\Delta = 2A|\zeta_8^z - \zeta_9^z| \simeq 3 \ \text{cm}^{-1}. \tag{44}$$

In Fig. 12 the Raman transitions are shown between the ζ^z-Coriolis split energy levels, with their torsional splittings and statistical weights. A fit of a simulated spectrum to the experimental one yielded the following constants:

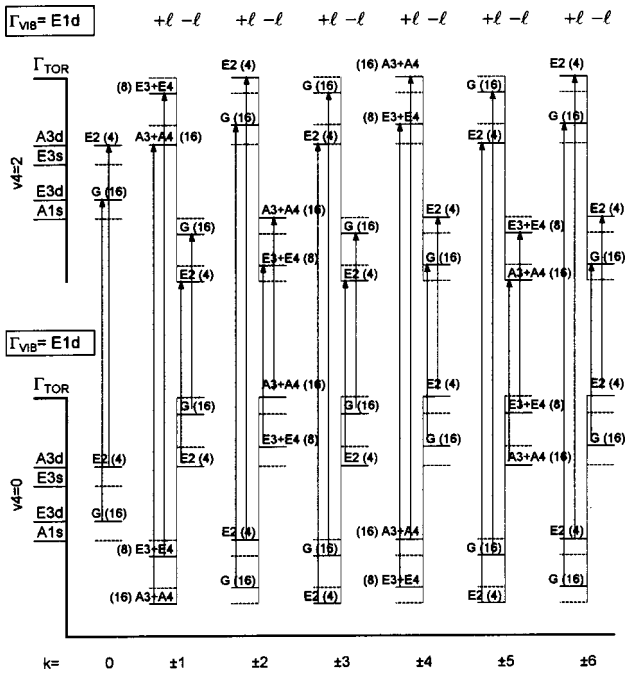

FIG. 12. Raman transitions for the $\nu_9 \rightarrow (\nu_8+2\nu_4)$ band. For the notation of vibrational–torsional–rotational energy levels and *z*-Coriolis splittings see the text and caption to Fig. 2.

$$(\nu_8+2\nu_4)=2014.08\pm 0.3 \ \ \mathrm{cm}^{-1}, \tag{45}$$

$$\zeta^z(\nu_8+2\nu_4)=-0.099\pm 0.008. \tag{46}$$

The simulated spectrum compares reasonably well with the experimental one, as shown in Fig. 9.

In addition, each ${}^{Q}Q_K$ branch should be split into one "*A*" and one "*E*" sub-branch, due to the large torsional splitting expected for the final state $(\nu_8+2\nu_4)$ with two quanta of torsional excitation. Assuming a torsional behavior in ν_8 like in the ground vibrational state, the splitting between A/E components is $\sim 3.9\ \mathrm{cm}^{-1}$, and would be noticeable even in the low resolution spectrum of Fig. 9. However, in the simulation of Fig. 9 no torsional splitting was included, which is an indication that in the combination state $(\nu_8+2\nu_4)$ it is smaller than expected.

There is some evidence in the literature that the torsional motion in degenerate vibrational states in ethanelike molecules is not as simple as in nondegenerate states. From the analysis[18] of the IR combination $(\nu_{11}+\nu_4)$, the torsional splitting in that state was found smaller than with the same torsional excitation in the ground vibrational state, and that was attributed to an increased barrier in the torsional potential. This problem has been treated in some detail by di Lauro *et al.*[43,35] In particular, they showed that the torsional splitting in those degenerate states is the combined effect of the torsional motion itself plus the interaction between pairs of degenerate vibrations from top and frame fragments. The torsional splitting is especially sensitive to those interactions when the Coriolis ζ^z constant is close to -0.5, the value where the torsional splitting tends to zero and changes sign, going from E_{1d}/E_{2d} description to a E_{1s}/E_{2s} one. The ν_8 and ν_{11} modes (HCH bendings) have ζ^z constant ~ -0.3. Thus, they conclude[43,35] that the observed small splitting in $(\nu_{11}+\nu_4)$ does not necessarily require an increase of the barrier, but can be due to the top/frame vibrational interactions, and the same can be said of the torsional combinations $\nu_8+n\nu_4$. This also could be the reason for the large change in the Coriolis ζ^z constant in ν_8 from the fundamental state (-0.3025) to two quanta torsional excitation (-0.099). It must be stressed that the Coriolis ζ^z constants in ethane pose an unsolved question, as recognized time ago,[44] since they do not satisfy the sum rule

$$\sum_{E_g,E_u} \zeta_i^z = B/2A, \tag{47}$$

for molecules with internal rotation.[29,45]

F. $\nu_7(E_{1d})$, $\nu_8(E_{1d})$, and $\nu_9(E_{1d})$ fundamental bands

Finally, the strong IR perpendicular bands ν_7, ν_8, and ν_9, deserve some comment. Contrary to what is expected from a superficial reading of the symmetry properties of the polarizability tensor in the character table of G_{36}^{+} group,[27] the fundamental bands ν_7, ν_8, and ν_9 of ethane, of symmetry E_{1d}, are Raman active according to selection rules number 1 and 5 in Table III. However, the intensity of the $\Delta k=\pm 2$ transitions, though depending on the non-neglegible coefficients M_7, M_8, and M_9 in Eq. (29), are weighted with the square of the very small transition moments $\langle 0E_{3s}|\cos 3\gamma|0E_{3d}\rangle$, given in Table V. On the other hand, the $\Delta k=\pm 1$ transitions are missing since transition moments $\langle v_4\sigma|\sin 6\gamma|v_4\sigma\rangle$ are zero by symmetry.

In summary, $\nu_7(E_{1d})$, $\nu_8(E_{1d})$, and $\nu_9(E_{1d})$ bands, though permitted by symmetry in the Raman spectrum of floppy ethane, may be expected to be exceedingly weak. Indeed, no evidence of these bands has been found under the present experimental conditions. But, this is not the case when the torsional potential barrier is much smaller, like in CH_3CCCH_3, as commented below.

IV. CONCLUDING REMARKS

We have shown the detailed selection rules for the Raman-active transitions in C_2H_6 from the ground state to a degenerate vibrational state, and between two degenerate vibrational states. In both cases, a complex structure of the rotational–torsional energy levels is involved. The Raman spectra of some bands of C_2H_6 concerning these transitions have been recorded with probably the best sensitivity available today. Spectra are reported for the three fundamental bands ν_{10}, ν_{11}, and ν_{12}, plus the degenerate combinations $\nu_7+\nu_4$, $(\nu_8+\nu_{11})(E)$, and the difference $(\nu_8+2\nu_4)-\nu_9$ involving two degenerate states.

In the case of the intense ν_{10} and ν_{11} bands, spectra have been also recorded at temperatures in the range 13–80 K in supersonic expansions of both pure C_2H_6 and mixtures with He. From these cold spectra the band origins have been unambiguously determined, as well as several molecular constants. The combinations $\nu_7+\nu_4$ and $(\nu_8+\nu_{11})(E)$ have been assigned for the first time on the basis of the spacing of the prominent ${}^{O,S}Q_K$ peaks, and the Coriolis ζ^z constants determined. The analysis of the region of the ν_{12} fundamental band have allowed to measure the ζ_{12}^z constant, to date

only indirectly known from the IR combination $\nu_{12}+\nu_4$. However, the strongest feature in this region has been shown to be $(\nu_8+2\nu_4)-\nu_9$, a (difference) totally symmetric band between two degenerate vibrational states, one of them with two quanta of torsional excitation.

Though current resolution has not been enough to reveal the efect of the torsional splittings in the recorded spectra, the theoretical background explained in the first part of the present paper will become essential to interpret higher resolution Raman spectra of the degenerate bands of ethane, in an analog way to those of the totally symmetric ν_3 and "ν_1+resonances" bands.[5,16] In the case of $(\nu_8+2\nu_4)-\nu_9$, the lack of these splittings, for a state with two quanta of torsional excitation, is a somewhat unexpected result. This, together with previous evidence from the literature, suggests strongly that the torsional motion in the degenerate vibrational states is more complex than in nondegenerate states.

The introduction of a torsionally dependent polarizability tensor allows one to reconcile the apparent contradiction of the Raman activity of the degenerate modes in going from D_{3d} to G_{36}^+ symmetry groups: the G_{36}^+ (floppy) model of ethane, a more accurate description, seemed to lose one component of the degenerate Raman vibrations in ethane, while the actual spectra show basically "D_{3d}-like" bands, i.e., whith *two* components. The operator responsible for the lost component has a $\sin 3\gamma$ torsional dependence; in turn, the IR active vibrations become Raman allowed through operators with torsional dependences of the form $\sin 6\gamma$ and $\cos 3\gamma$. This also allows one to trace a conceptual transition from a D_{3d} description to a G_{36}^+ one, through the Raman intensity of the degenerate modes: in ethane, where the torsional potential barrier is moderately high, the transition moments of the torsionally dependent operators between torsional levels within the potential well are $\simeq 1$ if $\Delta v_4=0$ for the Raman modes, while for the IR modes they are ~ 0 when $\Delta v_4=0$ and become only significantly different from 0 when $\Delta v_4=\pm 1$. As a result of the floppiness, part of the intensity of the $\Delta k=\pm 2$ component of D_{3d} ethane "leaks" into the IR vibration (appropriately combined with a change in the torsional excitation); the lower the barrier the greater the intensity transfer. In the limit case of D_{3h} eclipsed ethane, all the Raman intensity of the $\Delta k=\pm 2$ component occur with the E_{1d} "IR" mode.

A similar effect can be conceived for the IR intensity, through the torsional dependence of the dipole moment, but in this case no intensity is transferred from the E_{1d} IR-active mode to the E_{2d} Raman-active one (to the same level of approximation). For the E_{1d} vibration the dipole moment $\mu_{\pm 1}^{(1)}$ has a constant term plus a $\cos 6\gamma$ dependence, while for the E_{2d} vibration it has a $\sin 6\gamma$ modulation. This leads to a transition moment that vanishes by symmetry for the $\Delta v_4=0$ transitions, and no intensity will be observed in the IR spectrum for transitions to the levels of the Raman fundamental bands. Actually, to our knowledge, no weak absorption in the IR spectrum of C_2H_6 have been observed that could be attributed to the Raman modes ν_{10}, ν_{11}, or ν_{12}. The Raman-active vibrations become allowed in the IR in the form of combinations or differences with the torsion, but in this case the intensity comes from higher order terms, the equivalent to the g_i's in Eqs. (22) and (25), and thus no straightforward relation between the intensity of the IR fundamental band and that of the Raman combination can be derived.

Finally, it is also interesting to comment briefly on the case when the torsional motion is almost free, like in dimethylacetylene. This problem was already studied by Bunker and di Lauro,[46] though from a different point of view. This situation can be considered as intermediate between the two limiting cases of staggered (D_{3d}) and eclipsed (D_{3h}) models of ethane. Being closer to a free rotation than to a torsional oscillation, the transition moments in Table V of the torsional operators responsible for the Raman intensity are not as clearly defined (close to 0 or 1 depending on the value of Δv_4) as in ethane, but a lot of them will be significantly different from 0, independently of Δv_4. The intensity of the $\Delta k=\pm 2$ Raman transitions is expected to be split, in comparable amounts, between the two E_{1d} and E_{2d} modes, and the E_{1d} IR-active mode will be observed in the Raman spectrum (though with different rotational selection rules than in the IR), mixed with the close-lying E_{2d} Raman-active mode. As a result, the high resolution Raman spectrum of dimethylacetylene[46] is far more complex than in ethane.

ACKNOWLEDGMENTS

This work was supported by the Spanish DGICYT and DGES, research projects PB94-1526 and PB97-1203.

[1] J. Susskind, D. Reuter, D. E. Jennings, S. J. Daunt, W. Blass, and G. W. Halsey, J. Chem. Phys. **77**, 2728 (1982).
[2] L. Henry, A. Valentin, W. J. Lafferty, J. T. Hougen, V. M. Devi, P. P. Das, and K. N. Rao, J. Mol. Spectrosc. **100**, 260 (1983).
[3] S. J. Daunt, A. K. Atakan, W. E. Blass, G. W. Hasley, D. E. Jennings, D. C. Reuter, J. Susskind, and J. W. Brault, Astrophys. J. **280**, 921 (1984).
[4] N. Moazzen-Ahmadi, J. Mol. Spectrosc. **214**, 144 (2002).
[5] D. Bermejo, J. Santos, P. Cancio, J. M. Fernández-Sánchez, and S. Montero, J. Chem. Phys. **97**, 7055 (1992).
[6] J. Susskind, J. Mol. Spectrosc. **49**, 331 (1974).
[7] M. Hepp and M. Herman, J. Mol. Spectrosc. **194**, 1 (1999).
[8] A. S. Pine and W. J. Lafferty, J. Res. Natl. Bur. Stand. **87**, 237 (1982).
[9] A. R. H. Cole, K. J. Cross, J. A. Cughley, and H. M. Heise, J. Mol. Spectrosc. **83**, 233 (1980).
[10] A. S. Pine and S. C. Stone, J. Mol. Spectrosc. **175**, 21 (1996).
[11] F. Mélen, M. Herman, G. Y. Matti, and D. M. McNaughton, J. Mol. Spectrosc. **160**, 601 (1993).
[12] D. W. Lepard, D. E. Shaw, and H. L. Welsh, Can. J. Phys. **44**, 2353 (1966).
[13] J. Martín and S. Montero, J. Chem. Phys. **80**, 4610 (1984).
[14] L. G. Smith, J. Chem. Phys. **17**, 139 (1949).
[15] K. Van Helvoort, W. Knippers, R. Fantoni, and S. Stolte, Chem. Phys. **111**, 445 (1987).
[16] L. Abad, D. Bermejo, P. Cancio, C. Domingo, V. J. Herrero, J. Santos, I. Tanarro, and S. Montero, J. Raman Spectrosc. **25**, 589 (1994).
[17] J. M. Fernández-Sánchez, A. Valdenebro, and S. Montero, J. Chem. Phys. **91**, 3327 (1989).
[18] J. Susskind, J. Mol. Spectrosc. **49**, 1 (1974).
[19] W. E. Blass, G. W. Halsey, J. Susskind, D. C. Reuter, and D. E. Jennings, J. Mol. Spectrosc. **141**, 334 (1990).
[20] J. Susskind, L. Iredell, W. E. Blass, D. C. Reuter, W. G. Hasley, and D. E. Jennings, J. Mol. Spectrosc. **192**, 119 (1998).
[21] J. Oomens and J. Reuss, J. Mol. Spectrosc. **177**, 19 (1996).
[22] M. Hepp and M. Herman, Mol. Phys. **94**, 829 (1998).
[23] M. Hepp, R. Georges, and M. Herman, Chem. Phys. Lett. **275**, 513 (1997).
[24] C. Domingo and S. Montero, J. Chem. Phys. **86**, 6046 (1987).
[25] See, e.g., B. S. Galabov and T. Dudev, *Vibrational Intensities*, Vibrational

Spectra and Structure, Vol. 22 (Elsevier, Amsterdam, 1996), and references therein.
[26] E. N. Svendsen and T. Stroyer-Hansen, Mol. Phys. **56**, 1025 (1985).
[27] P. R. Bunker, *Molecular Symmetry and Spectroscopy* (Academic, San Diego, 1979).
[28] J. T. Hougen, J. Mol. Spectrosc. **82**, 92 (1980).
[29] P. R. Bunker, J. Chem. Phys. **47**, 718 (1967).
[30] J. T. Hougen, Can. J. Phys. **42**, 1920 (1964).
[31] R. Fantoni, K. Van Helvoort, W. Knippers, and J. Reuss, Chem. Phys. **110**, 1 (1986).
[32] N. Moazzen-Ahmadi, H. P. Gush, M. Halpern, H. Jagannath, A. Leung, and I. Ozier, J. Chem. Phys. **88**, 563 (1988).
[33] N. Moazzen-Ahmadi, A. R. W. McKellar, J. W. C. Johns, and I. Ozier, J. Chem. Phys. **97**, 3981 (1992).
[34] B. Kirtman, J. Chem. Phys. **40**, 390 (1963).
[35] F. Lattanzi and C. di Lauro, J. Mol. Spectrosc. **198**, 304 (1999).
[36] P. R. Bunker and J. T. Hougen, Can. J. Phys. **45**, 3867 (1967).
[37] F. Lattanzi, C. di Lauro, and N. Leguey-Sommaire, J. Mol. Spectrosc. **156**, 227 (1992).
[38] J. L. Duncan, R. A. Kelly, G. D. Nivellini, and F. Tullini, J. Mol. Spectrosc. **98**, 87 (1983).
[39] G. Tejeda, J. M. Fernández-Sánchez, and S. Montero, Appl. Spectrosc. **51**, 265 (1997).
[40] M. Loëte and H. Berger, J. Mol. Spectrosc. **68**, 317 (1977).
[41] A. Al-Kahtani, S. Montero, and J. Nibler, J. Chem. Phys. **98**, 101 (1993).
[42] J. Romanko, T. Feldman, and H. L. Welsh, Can. J. Phys. **33**, 588 (1955).
[43] C. di Lauro, F. Lattanzi, and R. Avellino, J. Mol. Spectrosc. **167**, 450 (1994).
[44] A. Weber, in *The Raman Effect*, edited by A. Anderson (Dekker, New York, 1973), Vol. 2.
[45] J. T. Hougen, Can. J. Phys. **43**, 935 (1965).
[46] P. R. Bunker and C. di Lauro, Chem. Phys. **190**, 159 (1995).